THE UNIVERSITY OF CALGARY

TRANSMISSION CHARACTERISTICS AND LOCALIZATION OF KNEE JOINT VIBROARTHROGRAPHIC SIGNALS

by

Yiping Shen

A THESIS

SUBMITTED TO THE FACULTY OF GRADUATE STUDIES

IN PARTIAL FULFILLMENT OF THE REQUIREMENTS FOR THE

DEGREE OF MASTER OF SCIENCE

DEPT. OF ELECTRICAL AND COMPUTER ENGINEERING

CALGARY, ALBERTA

DECEMBER, 1993

ISBN 0-315-93975-3

Name Yiping Shen

Dissertation Abstracts International is arranged by broad, general subject categories. Please select the one subject which most nearly describes the content of your dissertation. Enter the corresponding four-digit code in the spaces provided.

Biomedical Engineering
SUBJECT TERM

0541
SUBJECT CODE

U·M·I

Subject Categories

THE HUMANITIES AND SOCIAL SCIENCES

COMMUNICATIONS AND THE ARTS
Architecture 0729
Art History 0377
Cinema 0900
Dance 0378
Fine Arts 0357
Information Science 0723
Journalism 0391
Library Science 0399
Mass Communications 0708
Music 0413
Speech Communication 0459
Theater 0465

EDUCATION
General 0515
Administration 0514
Adult and Continuing 0516
Agricultural 0517
Art 0273
Bilingual and Multicultural 0282
Business 0688
Community College 0275
Curriculum and Instruction 0727
Early Childhood 0518
Elementary 0524
Finance 0277
Guidance and Counseling 0519
Health 0680
Higher 0745
History of 0520
Home Economics 0278
Industrial 0521
Language and Literature 0279
Mathematics 0280
Music 0522
Philosophy of 0998
Physical 0523
Psychology 0525
Reading 0535
Religious 0527
Sciences 0714
Secondary 0533
Social Sciences 0534
Sociology of 0340
Special 0529
Teacher Training 0530
Technology 0710
Tests and Measurements 0288
Vocational 0747

LANGUAGE, LITERATURE AND LINGUISTICS
Language
General 0679
Ancient 0289
Linguistics 0290
Modern 0291
Literature
General 0401
Classical 0294
Comparative 0295
Medieval 0297
Modern 0298
African 0316
American 0591
Asian 0305
Canadian (English) 0352
Canadian (French) 0355
English 0593
Germanic 0311
Latin American 0312
Middle Eastern 0315
Romance 0313
Slavic and East European 0314

PHILOSOPHY, RELIGION AND THEOLOGY
Philosophy 0422
Religion
General 0318
Biblical Studies 0321
Clergy 0319
History of 0320
Philosophy of 0322
Theology 0469

SOCIAL SCIENCES
American Studies 0323
Anthropology
Archaeology 0324
Cultural 0326
Physical 0327
Business Administration
General 0310
Accounting 0272
Banking 0770
Management 0454
Marketing 0338
Canadian Studies 0385
Economics
General 0501
Agricultural 0503
Commerce-Business 0505
Finance 0508
History 0509
Labor 0510
Theory 0511
Folklore 0358
Geography 0366
Gerontology 0351
History
General 0578
Ancient 0579
Medieval 0581
Modern 0582
Black 0328
African 0331
Asia, Australia and Oceania 0332
Canadian 0334
European 0335
Latin American 0336
Middle Eastern 0333
United States 0337
History of Science 0585
Law 0398
Political Science
General 0615
International Law and Relations 0616
Public Administration 0617
Recreation 0814
Social Work 0452
Sociology
General 0626
Criminology and Penology 0627
Demography 0938
Ethnic and Racial Studies 0631
Individual and Family Studies 0628
Industrial and Labor Relations 0629
Public and Social Welfare 0630
Social Structure and Development 0700
Theory and Methods 0344
Transportation 0709
Urban and Regional Planning 0999
Women's Studies 0453

THE SCIENCES AND ENGINEERING

BIOLOGICAL SCIENCES
Agriculture
General 0473
Agronomy 0285
Animal Culture and Nutrition 0475
Animal Pathology 0476
Food Science and Technology 0359
Forestry and Wildlife 0478
Plant Culture 0479
Plant Pathology 0480
Plant Physiology 0817
Range Management 0777
Wood Technology 0746
Biology
General 0306
Anatomy 0287
Biostatistics 0308
Botany 0309
Cell 0379
Ecology 0329
Entomology 0353
Genetics 0369
Limnology 0793
Microbiology 0410
Molecular 0307
Neuroscience 0317
Oceanography 0416
Physiology 0433
Radiation 0821
Veterinary Science 0778
Zoology 0472
Biophysics
General 0786
Medical 0760

EARTH SCIENCES
Biogeochemistry 0425
Geochemistry 0996
Geodesy 0370
Geology 0372
Geophysics 0373
Hydrology 0388
Mineralogy 0411
Paleobotany 0345
Paleoecology 0426
Paleontology 0418
Paleozoology 0985
Palynology 0427
Physical Geography 0368
Physical Oceanography 0415

HEALTH AND ENVIRONMENTAL SCIENCES
Environmental Sciences 0768
Health Sciences
General 0566
Audiology 0300
Chemotherapy 0992
Dentistry 0567
Education 0350
Hospital Management 0769
Human Development 0758
Immunology 0982
Medicine and Surgery 0564
Mental Health 0347
Nursing 0569
Nutrition 0570
Obstetrics and Gynecology 0380
Occupational Health and Therapy 0354
Ophthalmology 0381
Pathology 0571
Pharmacology 0419
Pharmacy 0572
Physical Therapy 0382
Public Health 0573
Radiology 0574
Recreation 0575
Speech Pathology 0460
Toxicology 0383
Home Economics 0386

PHYSICAL SCIENCES

Pure Sciences
Chemistry
General 0485
Agricultural 0749
Analytical 0486
Biochemistry 0487
Inorganic 0488
Nuclear 0738
Organic 0490
Pharmaceutical 0491
Physical 0494
Polymer 0495
Radiation 0754
Mathematics 0405
Physics
General 0605
Acoustics 0986
Astronomy and Astrophysics 0606
Atmospheric Science 0608
Atomic 0748
Electronics and Electricity 0607
Elementary Particles and High Energy 0798
Fluid and Plasma 0759
Molecular 0609
Nuclear 0610
Optics 0752
Radiation 0756
Solid State 0611
Statistics 0463

Applied Sciences
Applied Mechanics 0346
Computer Science 0984
Engineering
General 0537
Aerospace 0538
Agricultural 0539
Automotive 0540
Biomedical .... 0541 ✓
Chemical 0542
Civil 0543
Electronics and Electrical 0544
Heat and Thermodynamics 0348
Hydraulic 0545
Industrial 0546
Marine 0547
Materials Science 0794
Mechanical 0548
Metallurgy 0743
Mining 0551
Nuclear 0552
Packaging 0549
Petroleum 0765
Sanitary and Municipal 0554
System Science 0790
Geotechnology 0428
Operations Research 0796
Plastics Technology 0795
Textile Technology 0994

PSYCHOLOGY
General 0621
Behavioral 0384
Clinical 0622
Developmental 0620
Experimental 0623
Industrial 0624
Personality 0625
Physiological 0989
Psychobiology 0349
Psychometrics 0632
Social 0451

Nom ____

Dissertation Abstracts International est organisé en catégories de sujets. Veuillez s.v.p. choisir le sujet qui décrit le mieux votre thèse et inscrivez le code numérique approprié dans l'espace réservé ci-dessous.

____ [ ][ ][ ][ ] U·M·I

SUJET CODE DE SUJET

Catégories par sujets

HUMANITÉS ET SCIENCES SOCIALES

COMMUNICATIONS ET LES ARTS
Architecture 0729
Beaux-arts 0357
Bibliothéconomie 0399
Cinéma 0900
Communication verbale 0459
Communications 0708
Danse 0378
Histoire de l'art 0377
Journalisme 0391
Musique 0413
Sciences de l'information 0723
Théâtre 0465

ÉDUCATION
Généralités 515
Administration 0514
Art 0273
Collèges communautaires 0275
Commerce 0688
Économie domestique 0278
Éducation permanente 0516
Éducation préscolaire 0518
Éducation sanitaire 0680
Enseignement agricole 0517
Enseignement bilingue et multiculturel 0282
Enseignement industriel 0521
Enseignement primaire. 0524
Enseignement professionnel 0747
Enseignement religieux 0527
Enseignement secondaire 0533
Enseignement spécial 0529
Enseignement supérieur 0745
Évaluation 0288
Finances 0277
Formation des enseignants 0530
Histoire de l'éducation 0520
Langues et littérature 0279
Lecture 0535
Mathématiques 0280
Musique 0522
Orientation et consultation 0519
Philosophie de l'éducation 0998
Physique 0523
Programmes d'études et enseignement 0727
Psychologie 0525
Sciences 0714
Sciences sociales 0534
Sociologie de l'éducation 0340
Technologie 0710

LANGUE, LITTÉRATURE ET LINGUISTIQUE
Langues
- Généralités 0679
- Anciennes 0289
- Linguistique 0290
- Modernes 0291

Littérature
- Généralités 0401
- Anciennes 0294
- Comparée 0295
- Mediévale 0297
- Moderne 0298
- Africaine 0316
- Américaine 0591
- Anglaise 0593
- Asiatique 0305
- Canadienne (Anglaise) 0352
- Canadienne (Française) 0355
- Germanique 0311
- Latino-américaine 0312
- Moyen-orientale 0315
- Romane 0313
- Slave et est-européenne 0314

PHILOSOPHIE, RELIGION ET THÉOLOGIE
Philosophie 0422
Religion
- Généralités 0318
- Clergé 0319
- Études bibliques 0321
- Histoire des religions 0320
- Philosophie de la religion 0322

Théologie 0469

SCIENCES SOCIALES
Anthropologie
- Archéologie 0324
- Culturelle 0326
- Physique 0327

Droit 0398
Économie
- Généralités 0501
- Commerce-Affaires 0505
- Économie agricole 0503
- Économie du travail 0510
- Finances 0508
- Histoire 0509
- Théorie 0511

Études américaines 0323
Études canadiennes 0385
Études féministes 0453
Folklore 0358
Géographie 0366
Gérontologie 0351
Gestion des affaires
- Généralités 0310
- Administration 0454
- Banques 0770
- Comptabilité 0272
- Marketing 0338

Histoire
- Histoire générale 0578
- Ancienne 0579
- Médiévale 0581
- Moderne 0582
- Histoire des noirs 0328
- Africaine 0331
- Canadienne 0334
- États-Unis 0337
- Européenne 0335
- Moyen-orientale 0333
- Latino-américaine 0336
- Asie, Australie et Océanie 0332

Histoire des sciences 0585
Loisirs 0814
Planification urbaine et régionale 0999
Science politique
- Généralités 0615
- Administration publique 0617
- Droit et relations internationales 0616

Sociologie
- Généralités 0626
- Aide et bien-àtre social 0630
- Criminologie et établissements pénitentiaires 0627
- Démographie 0938
- Études de l' individu et de la famille 0628
- Études des relations interethniques et des relations raciales 0631
- Structure et développement social 0700
- Théorie et méthodes. 0344
- Travail et relations industrielles 0629

Transports 0709
Travail social 0452

SCIENCES ET INGÉNIERIE

SCIENCES BIOLOGIQUES
Agriculture
- Généralités 0473
- Agronomie. 0285
- Alimentation et technologie alimentaire 0359
- Culture 0479
- Élevage et alimentation 0475
- Exploitation des péturages 0777
- Pathologie animale 0476
- Pathologie végétale 0480
- Physiologie végétale 0817
- Sylviculture et faune 0478
- Technologie du bois 0746

Biologie
- Généralités 0306
- Anatomie 0287
- Biologie (Statistiques) 0308
- Biologie moléculaire 0307
- Botanique 0309
- Cellule 0379
- Écologie 0329
- Entomologie 0353
- Génétique 0369
- Limnologie 0793
- Microbiologie 0410
- Neurologie 0317
- Océanographie 0416
- Physiologie 0433
- Radiation 0821
- Science vétérinaire 0778
- Zoologie 0472

Biophysique
- Généralités 0786
- Medicale 0760

SCIENCES DE LA TERRE
Biogéochimie 0425
Géochimie 0996
Géodésie 0370
Géographie physique 0368
Géologie 0372
Géophysique 0373
Hydrologie 0388
Minéralogie 0411
Océanographie physique 0415
Paléobotanique 0345
Paléoécologie 0426
Paléontologie 0418
Paléozoologie 0985
Palynologie 0427

SCIENCES DE LA SANTÉ ET DE L'ENVIRONNEMENT
Économie domestique 0386
Sciences de l'environnement 0768
Sciences de la santé
- Généralités 0566
- Administration des hipitaux 0769
- Alimentation et nutrition 0570
- Audiologie 0300
- Chimiothérapie 0992
- Dentisterie 0567
- Développement humain 0758
- Enseignement 0350
- Immunologie 0982
- Loisirs 0575
- Médecine du travail et thérapie 0354
- Médecine et chirurgie 0564
- Obstétrique et gynécologie 0380
- Ophtalmologie 0381
- Orthophonie 0460
- Pathologie 0571
- Pharmacie 0572
- Pharmacologie 0419
- Physiothérapie 0382
- Radiologie 0574
- Santé mentale 0347
- Santé publique 0573
- Soins infirmiers 0569
- Toxicologie 0383

SCIENCES PHYSIQUES
Sciences Pures

Chimie
- Genéralités 0485
- Biochimie 487
- Chimie agricole 0749
- Chimie analytique 0486
- Chimie minérale 0488
- Chimie nucléaire 0738
- Chimie organique 0490
- Chimie pharmaceutique 0491
- Physique 0494
- PolymÇres 0495
- Radiation 0754

Mathématiques 0405
Physique
- Généralités 0605
- Acoustique 0986
- Astronomie et astrophysique 0606
- Electronique et électricité 0607
- Fluides et plasma 0759
- Météorologie 0608
- Optique 0752
- Particules (Physique nucléaire) 0798
- Physique atomique 0748
- Physique de l'état solide 0611
- Physique moléculaire 0609
- Physique nucléaire 0610
- Radiation 0756

Statistiques 0463

Sciences Appliqués Et Technologie

Informatique 0984
Ingénierie
- Généralités 0537
- Agricole 0539
- Automobile 0540
- Biomédicale 0541
- Chaleur et ther modynamique 0348
- Conditionnement (Emballage) 0549
- Génie aérospatial 0538
- Génie chimique 0542
- Génie civil 0543
- Génie électronique et électrique 0544
- Génie industriel 0546
- Génie mécanique 0548
- Génie nucléaire 0552
- Ingénierie des systämes 0790
- Mécanique navale 0547
- Métallurgie 0743
- Science des matériaux 0794
- Technique du pétrole 0765
- Technique minière 0551
- Techniques sanitaires et municipales 0554
- Technologie hydraulique 0545

Mécanique appliquée 0346
Géotechnologie 0428
Matières plastiques (Technologie) 0795
Recherche opérationnelle 0796
Textiles et tissus (Technologie) 0794

PSYCHOLOGIE
Généralités 0621
Personnalité 0625
Psychobiologie 0349
Psychologie clinique 0622
Psychologie du comportement 0384
Psychologie du développement 0620
Psychologie expérimentale 0623
Psychologie industrielle 0624
Psychologie physiologique 0989
Psychologie sociale 0451
Psychométrie 0632

THE UNIVERSITY OF CALGARY

FACULTY OF GRADUATE STUDIES

The undersigned certify that they have read, and recommend to the Faculty of Graduate Studies for acceptance, a thesis entitled, "**Transmission Characteristics and Localization of Knee Joint Vibroarthrographic Signals**", submitted by YIPING SHEN in partial fulfillment of the requirements for the degree of Master of Science.

Supervisor, Dr. R.M. Rangayyan
Dept. of Electrical and Computer Engineering

Dr. W.C. Chan
Dept. of Electrical and Computer Engineering

Dr. R.C. Bray
Dept. of Surgery

Date: 94.01.17

ABSTRACT

This thesis proposes non-invasive techniques to localize vibroarthrographic (VAG) signal sources and model vibration transmission characteristics of human knee joints. VAG signals from normal subjects, patients, and cadavers, obtained by stimulation with a finger tap over the mid-patella and swinging movement of the leg were analyzed for time delays using cross-correlation functions for source localization. Correct results were obtained for 13 of the 14 subjects tested by finger stimulation, and for 11 of the 12 subjects whose VAG signals during swinging movement were analyzed. VAG signals in response to finger stimulation were also used to study transmission characteristics. Models of frequency response functions derived indicate that the human knee behaves like a bandpass filter in the range 5 - 300 Hz with a peak between 30 Hz and 60 Hz. The techniques could be valuable in diagnosis and treatment of knee pathology and in joint surgery.

ACKNOWLEDGMENTS

I would like to express my sincere appreciation to Dr. Rangaraj Rangayyan, my supervisor, for his constructive suggestions, kind guidance, and encouragement provided during the entire course of this work.

I would also like to thank Dr. Cy Frank and Dr. Doug Bell for their guidance in areas related to knee joint injuries and their support in providing subjects, without which this work would have been impossible.

I appreciate Dr. Yuanting Zhang's and Mrs. Katherine Ladly's contributions to this research in data collection and providing clinical information. They also shared their experience and knowledge with me.

Finally, a very special thanks to my husband Liang Shen for his technical support during the entire work of this thesis.

Dedicated to

my parents

and

my family Liang and Jenny

TABLE OF CONTENTS

LIST OF TABLES

LIST OF FIGURES

CHAPTER 1

INTRODUCTION

The knee is the most commonly injured joint in the body. It has been indicated that knee injuries account for more than 65% of orthopaedic consultations [1]. Currently, accurate diagnosis is difficult without the expensive and semi-invasive techniques of arthrography and arthroscopy, especially during early stages of cartilage deterioration. Many studies have been directed towards the development of non-invasive diagnostic methods, with reported accuracy rates approaching that of arthrography. One such promising technique is based upon analysis of knee joint sound or vibration signals (known as vibroarthrographic or VAG signals), aimed at detecting knee joint problems before arthritis becomes clinically apparent.

This chapter presents a review of the anatomy, biomechanics, and physiology of the knee joint with particular reference to causes of sound production in the knee joint. A review of knee joint sound signal analysis is then provided, leading to details of organization of the thesis.

1.1 Anatomy and Physiology of the Knee Joint

The knee transmits loads, participates in motion, aids in conservation of momentum, and provides a force couple for activities involving the leg. The human knee joint is the largest and perhaps the most complex joint in the body. It is a synovial joint with four distinguishing features: a joint cavity, articular cartilage, a synovial membrane, and a fibrous capsule. It is a two-joint structure composed of the tibiofemoral joint and the patellofemoral joint; the former is between the tibia and the femur, and the latter is between the patella and the femur[2].

As illustrated in Fig. 1.1 [3], the bones involved in the knee joint are the femur, the tibia, and the patella. Two layers of articular cartilage cover the bone ends and let the knee bend and move smoothly. Two menisci, which are thick pads of cartilage, act as mobile buffers with a circumferential arrangement of collagen fibers that suits them to their weight-bearing, shock-absorbing function [4]. The surrounding muscles and ligaments offer strength and support the stability of the knee joint. The configurations of the articular surfaces are the large curved condyles of the femur, the flattened condyles of the tibia, and the facets of the patella. A synovial membrane lines the inner aspect of the fibrous capsule and extends to the edges of the articulating cartilages of the tibia and superiorly into the suprapatellar bursa of the femur. This bursa lies between the femur and the quadriceps tendon and is an extension of the joint cavity. The knee joint is located between the human body's two longest lever arms, which makes it particularly susceptible to injury.

The principal movements occurring at the knee joint are flexion and extension of the leg, but some medial and lateral rotation also occurs. Kinematics defines the range of motion and describes the surface joint motion in three planes: frontal (coronal or longitudinal), sagittal, and transverse (horizontal) [2]. The maximum flexion-extension range of the knee is up to approximately 150 degrees around the transverse axis. During knee extension, quadriceps force is required to extend the knee against increasing resistance [5]. The quadriceps force rises during the initial phase in knee extension and remains nearly constant at an average value of 177 Newtons between 50 and 15 degrees. When the extension is past 15 degrees, it rises rapidly, reaching an average of 350 Newtons at zero degree of extension [5]. During flexion of the knee joint, the stability of the patella depends on the tension of the quadriceps muscle until it moves into the trochlea of the femur. This is reported to occur between 15 and 20 degrees of flexion [6]. During the first 20 degrees of flexion, the tibia rotates medially, which decreases the quadriceps angle (the angle between the line of pull of the quadriceps and the patellar tendon) as the patella enters the trochlea from a lateral position. After 30 degrees of flexion, the patella is firmly compressed against the trochlea of the femur because of forces acting perpendicular to the patellofemoral articulation.

Although the knee joint is well constructed and is one of the strongest joints, its function is commonly deranged (e.g. in body contact sports such as hockey and football). There are many disorders associated with the knee joint due to a variety of traumatic and non-traumatic causes. Damages to the articular cartilage and the menisci are two of the most common knee injuries. Injuries associated with the menisci might occur because of tearing, splitting, or fraying of the shock-absorbing pads of the cartilage in the knee. A common condition is known as "chondromalacia patella" (soft cartilage of the patella), in which articular cartilage softens, fibrillates, and sheds off the undersurface of the patella. Similarly, wear and tear of the femorotibial articular cartilage surfaces is another common problem found with the knee, which results in rough joint surfaces. These pathologies may cause symptoms of pain and swelling, and eventually exhibit some associated sounds or VAG signals from the knee.

Vibrations or sounds emitted from human joints during their relative movements could be associated with pathological conditions in the knee joint, and may be useful indicators of roughness, softening, or the state of lubrication of the articular cartilage surfaces. Such externally detected sounds or vibration signals may therefore provide a useful non-invasive index of early degeneration or joint disease. The concept behind the identification of the injuries mentioned above, based on the analysis of knee joint vibration, is that signals of different characteristics are expected when joint surfaces are rough as compared to those when they are smooth and normal.

1.2 Review of Knee Joint Vibration Analysis

Many researchers have studied human knee VAG signals or sounds. As early as the 17th century, Robert Hooke first used auscultation to listen to joint sounds and suggested that joint noise could be used as a diagnostic sign in patients suffering from painful joints [7]. Blodgett [8] noticed the apparent sounds in normal joints and their changes with repetitive motion. He concluded that sound increased with age but was absent when effusion was present. Bircher, in 1913, reported that each type of meniscal injury could cause a distinctive sound signal [9]. Walters evaluated joint auscultation in 1929 [10], recording joint sounds of 1600 patients. The joint sounds were graded and correlated with presumed pathology. He noted that the sounds were helpful in the diagnosis of painful joints with limited physical findings and normal "skiagrams". These studies were expanded by Erb in 1933, who was the first to attempt to use electronic and graphic recording of the knee joint sound signal using a contact microphone, and recorded the sound signal on paper in the form of a graph [11]. In 1937, Steindler used a cardiophone, an oscilloscope, and a recorder to record knee sound signals [12]. His study was the first one to record joint angle and the first one to remove noise and improve the signal using filters. Peylan used a regular stethoscope and an electronic stethoscope to study several types of arthritis in 214 patients [13]. A significant goal of his research was to distinguish between periarticular sounds, osteoarthritis, and rheumatoid arthritis. Fischer and Johnson observed that sound signals produced by normal knee joints have different characteristics compared to joints with degenerative arthritis or rheumatoid arthritis. Their results showed that sound signals could be detected in rheumatoid arthritis before x-ray changes were observable [14]. Szabo et al. [15] reported on the analysis of acoustic signals recorded from 240 patients, with the results of classification into six groups.

The group led by Chu at Ohio published a series of papers on the analysis of joint sounds in the 1970's [16, 17, 18, 19]. Their studies included methods to reduce extrinsic sounds, such as noise due to snapping tendons, hand tremor, skin friction, and other background noise; the use of statistical parameters such as autocorrelation function of the knee sound signal for classification of signals; and the relationship between signal acoustic power and articular cartilage damage (surface roughness) [17, 18].

Recently, Mollan and his co-workers in Northern Ireland published a series of papers on the nature of knee joint signals, their diagnostic potential, as well as the problems encountered in practice [20, 21, 22, 23, 24, 25] . They performed experiments on the type of recording system to be used for recording of knee joint vibration signals, and concluded that contact vibration (acceleration) sensors are better suited than acoustic transducers [22, 25] because the lower frequencies present in the signals are missed by the acoustic microphones but are recorded by contact sensors. They found that 86% of the patients (150 out of 247 patients on whom arthroscopy was performed) with meniscal injuries produced characteristic signals [24], and that alterations in normal joint crepitus may be useful indicators of early cartilage degeneration. They also found that the signal was largest on the affected side, had a large displacement, and appeared repetitively at the same knee angle in cycles. They reported that bizarre, irregular signals were produced in the range $300 - 600$ Hz by degenerate articular cartilage.

Mang et al. [26] also reported on the analysis of knee joint sound signals. Based upon the division of sound peaks into frequency groups, this team was apparently able to identify by sound analysis clinically and operatively demonstrated chondromalacia patella, meniscus lesions, and arthritis. Inoue et al. published the results of frequency analysis of knee sound signals using a narrow-band spectrum analyzer and a computer, and discussed procedures for the reduction of noise in the recording of knee joint sounds [27, 28].

Studies on the recording and analysis of knee joint vibration signals at The University of Calgary started in the summer of 1986 [29]. The purpose of the work of this group is to develop an objective, non-invasive tool for early detection, monitoring, and localization of both articular cartilage and meniscus pathology in the human knee joint by analyzing VAG signals. A microcomputer system developed earlier for the analysis of the phonocardiogram was modified to pre-process the knee joint vibration and angle signals [29]. A paper by Zhang et al. [30] reported on muscle contraction interference in recording knee vibration signals, and the use of adaptive filtering techniques to reduce this interference is being investigated [31]. A comparative study of normal and abnormal knee sound signals and muscle signals based on their differences in the time and frequency domains was reported by Ladly in 1992 [32]. It was reported that sound signals due to contraction of muscle could be a large source of variance to the knee sound signals. The technique of adaptive segmentation and modeling based on linear prediction (LP) was explored by Tavathia et al. [33]. Two features - the dominant pole and the average power of the model of each segment - were used to classify the signals to four groups. This technique was further developed by Moussavi et al. [34]: the signals from 7 normal subjects and 6 patients who underwent arthroscopy were segmented by adaptive modeling to 148 segments and classified using linear prediction and other parameters. The overall accuracy of classification was 83.78% [34].

Many investigations on knee vibrations or sounds have been carried out in the past few years, and the relation between VAG signals and knee pathology has been demonstrated. There is very good evidence to suggest that the analysis of knee joint vibration signals has an exciting potential for distinguishing between normal and abnormal cartilage surfaces. However, almost all of these studies used single-channel signal analysis techniques, and consequently they could not indicate the location of the pathology, although such information is important for the development of a non-invasive tool for diagnosis of pathology in the human knee joint. Correct and accurate source localization could provide useful information concerning the part of the knee joint which is affected or injured, which could be valuable in joint surgery and the monitoring of joint disease. There is a need to develop methods for source localization, which could be achieved using cross-spectrum, event estimation, and time delay analysis of multi-channel VAG signals. These techniques could make it possible to infer the part of the knee causing a VAG component. Quantitative features such as amplitude, attenuation factor, frequency peaks, durations of signal components, and bandwidth may aid in source localization. Time delays among different channels are related to transfer characteristics, such as velocity and transfer function. Therefore, the study of frequency response functions for various paths of sound transmission could be useful in localization.

The purpose of this thesis is to develop an objective, non-invasive method for localization of various types of knee VAG signals using multi-channel signal analysis techniques. Transfer characteristics, cross-spectrum, and time delay analysis techniques are applied to multi-channel VAG data in order to explore the possibility of localization of vibration sources to within the various natural or clinically relevant partitions or compartments of the knee joint.

1.3 Thesis Outline

The thesis is organized into 7 chapters. Chapter 2 discusses VAG data acquisition methods. The equipment used and the acquisition procedure to record knee joint vibration signals are described. Arthroscopy and auscultation are also briefly described due to their use to verify the results of VAG signal analysis for source localization. Three types of signals: one from a normal subject, one from a cadaver with arthroscopically-created lesions, and one from a patient with cartilage pathology, are presented in this chapter; these signals are used as running examples throughout the thesis to illustrate the results obtained by the various methods.

The signal processing techniques and applicatioins used for analysis of transmission characteristics are discussed in chapter 3. The theory and methods of transfer function estimation are presented.

Chapter 4 is concentrated on time delay estimation for source localization. In particular, methods of coherence, cross-correlation, bearing and range estimation and adaptive time delay estimation for analyzing multi-channel signals, as well as their applications for source localization are introduced.

The potential use of transfer characteristics and source localization with knee joint vibration signals is investigated in chapter 5 and chapter 6. Some experimental results are illustrated in the corresponding chapters.

Finally, the clinical relevance, usefulness, and limitations of the methods presented in this thesis are discussed in chapter 7, which concludes the thesis with recommendations and directions for future work.

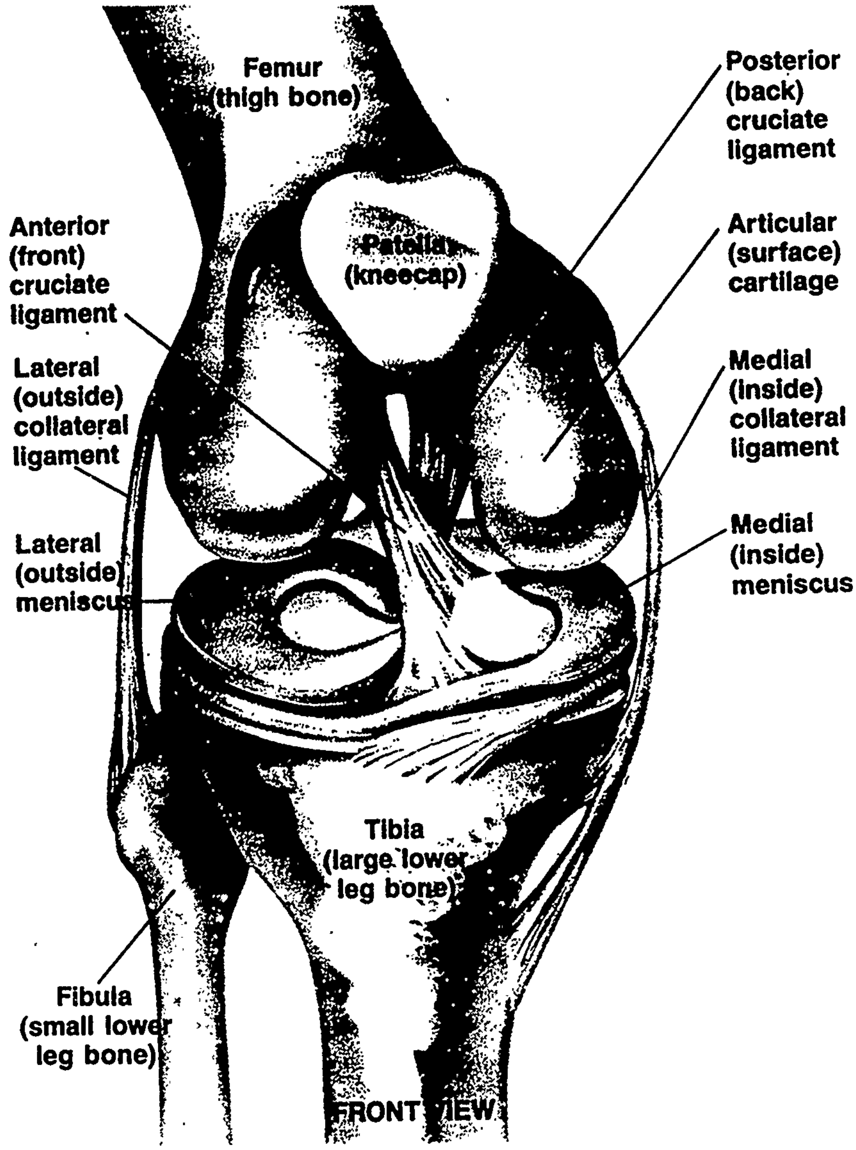

Figure 1.1 Anterior view of the right knee joint: The patella is reflected up to allow the posterior surface of the patella to be seen. The knee ligaments include the medial (MCL) and lateral (LCL) collateral ligaments, and the anterior (ACL) and posterior (PCL) cruciate ligaments [3]. (From Krames Communications with permissions.)

CHAPTER 2

VIBROARTHROGRAPHIC SIGNAL ACQUISITION

2.1 Multi-channel Signal Acquisition

A multi-channel acceleration VAG signal recording system has been established at The University of Calgary using four miniature accelerometers (Dytran 3115A), four Gould isolation pre-amplifiers (model 11-5407-58), four Gould channel-selective universal amplifiers (model 13-4615-58), and a Zenith PC 386 computer as shown in Fig. 2.1. Filters with the universal amplifier were set to have bandpass characteristics with a bandwidth of 10 Hz to 1 kHz to minimize low-frequency movement artifacts and high-frequency transducer noise although there could be some VAG signal components beyond this frequency range. The accuracy and reliability of this system were tested initially using known signals produced by a standard vibration signal generator, and then by in vivo tests on three human subjects by a multiple test-retest protocol.

2.2 Sensors and their Positions on the Knee Joint

As mentioned above, four Dytran vibration transducers (model 3115A) are used in the multi-channel vibration detection system. The reasons for using this accelerometer for VAG measurement are its small size (diameter 0.62 cm and height 0.58 cm), and light weight (1.5 grams), which minimize possible load effects and artifacts associated with attachment on the knee joint. The model 3115A piezoelectric accelerometer utilitzes quartz crystals and a preloaded seismic mass to generate a voltage signal exactly analagous to acceleration into its base. The output frequency response at $+/-$ 3 dB is: 0.66 Hz to 12 kHz; the output sensitivity is 10 mV/G (units of gravity).

In the recording experiments, four miniature accelerometers were stuck on to the skin surface of the knee joint using two-sided adhesive tape. The four positions used are: mid-patella (MP), lateral condyle (LC), medial condyle (MC), and tibial tuberosity (TT). The transducer on the mid-patella is expected to provide information on the patellofemoral joint. The VAG signal is expected to be strong at the MP position if the subject has chondral pathology. If the source is in the tibiofemoral joint such as meniscal pathology, the VAG signal may be strong at MC, LC, or TT. For this reason three transducers are placed at the MC, LC, and TT positions individually.

An electrogoniometer is attached to the lateral aspect of the knee, centered at the axis of knee rotation, in order to record joint angle.

2.3 Subjects and Experiments

Three types of subjects were involved in this study: normal subjects who were volunteers; patients who had joint pathology and were tested just prior to arthroscopy; and cadavers with lesions created by arthroscopy.

Normal subjects and patients were seated at the edge of a table, and asked to swing their legs through flexion-extension cycles at a constant angular velocity of 4 seconds per swing cycle (a swing is defined as movement from 0^o to about 135^o and back to the 0^o position), while keeping their muscles relaxed in order to reduce the effect of muscle contraction interference. Auscultation was performed using a stethoscope positioned on the medial, lateral, and anterior aspects of the knee. The sounds heard were documented according to the joint angle band they were heard in and the type of sound produced, such as grinding, click, pop, and clunk.

The patients who participated in the recording of VAG signals were scheduled to undergo arthroscopy independent of this study. Arthroscopy is a surgical procedure which allows the surgeon to look directly into the knee and diagnose most problems. The arthroscopy shaft contains a series of magnifying lenses and coated glass fibers that beam an intense, cool light into the joint and relay a magnified image to the viewer. A television monitor is used to give the surgeon a clear view and facilitate access to most areas of the joint. The arthroscope is inserted through tiny incisions called portals. Most problems can be diagnosed accurately and usually treated surgically at the same time. The high diagnostic accuracy of arthroscopy has led us to use it to verify the results of signal processing for localization.

Fresh cadaver knee joints were also used for recording VAG signals in this study. The purpose of using cadaver knees is to study the nature of VAG signals caused by lesions of known characteristics created using arthroscopic tools. The quadriceps tendon of the cadaver knee under investigation was exposed and connected to a hydraulic actuator system through a cable. Force was applied to the tendon in the direction of the quadriceps muscles by an electro-mechanical actuator connected to a mechanical linkage that consisted of a pulley and force sensor attached to each other by a cable. The patello-femoral tendon was attached to this cable and its force was measured with the force transducer in series. The entire actuator system was connected to a computer, and the patterns of knee movement and angular velocity were maintained under the precise control of the computer. A motorized arthroscopic shaver system was used to create localized cartilage lesions in the patello-femoral joint and then the tibio-femoral joint, first as partial thickness cartilage loss and then as full thickness cartilage loss.

2.4 Signal Recording and Examples

Two types of VAG signals are investigated in this study: one due to external stimulation by a finger tap, and the other during swinging movement. VAG signals obtained by stimulating with a finger tap were tape-recorded immediately following clinical auscultation. VAG signals during swinging movement were then recorded as the second kind of signals. The VAG signals picked up by the transducers were pre-amplified using the Gould isolation pre-amplifier, passed through the Gould channel-selective universal amplifier with the filter range of 10 Hz to 1 kHz, and recorded on a Hewlett Packard (HP) instrumentation recorder (model 3968A) along with the goniometer signal. The recorded signals were digitized with a sampling rate of 15 kHz and 12 bits/sample by using a National Instruments AT-MIO-16L signal data acquisition board and Labwindows software on a Zenith 386 computer. The signal from the goniometer was converted to real angle (0^o–135^o) based on the voltage of the goniometer at 0^o and 90^o. The digitized signals were then used to produce time domain plots of the VAG signals and the corresponding angle values.

Normalization of the VAG signals by the amplifier gain used in recording and multiplying by a common factor to convert the digitized voltage into acceleration units make VAG signals of different subjects directly comparable.

2.4.1 VAG Signals due to Stimulation

A single-finger tap over the upper-pole of the patella was used to elicit VAG signals from the normal and abnormal subjects while they were seated on the test table with the leg relaxed in the 90^o position. VAG signals produced by the stimulation were recorded using the multi-channel vibration recording system as described above. VAG signals were obtained in the same manner for cadavers as well, with the leg angle (90^o)

controlled by the hydraulic actuator system.

Fig. 2.2 illustrates a set of VAG signals obtained from a normal subject in response to a tap. A peak and its propagation wave are seen on each channel. The amplitude of the signal from the mid-patella (MP) is the largest, and it presents at the earliest instant. This corresponds to the tap signal source, which is on the upper-pole of the patella. The amplitude of the signal at MC is very small due to the transmission properties of the knee. The signal of the goniometer is almost constant as the angle of the leg was kept at 90^o.

2.4.2 VAG Signals During Swinging Movement

The subjects were asked to swing their legs at a period of 4 seconds per swing for recording the second type of VAG signals. Fig. 2.3 shows the time domain plots corresponding to a set of VAG signals obtained during swinging movement from a patient who had lateral chondromalacia and medial patella chondromalacia. A click is observed at each position at about 0.03 seconds. The output voltage of the goniometer did not change much over the short time period represented by the plots.

For recording VAG signals from cadavers, extension and flexion were controlled at rates and ranges similar to those established for in vivo vibration recording (4 seconds per swing). One set of representative signals obtained from a cadaver during swinging movement after a cartilage lesion was arthroscopically induced in the knee joint is showed in Fig. 2.4. The clicks seen are due to a deep lesion cut near the mid-patella during arthroscopy. The absence of a recordable VAG signal at the lateral condyle could be due to the transmission characteristics of the particular cadaver knee.

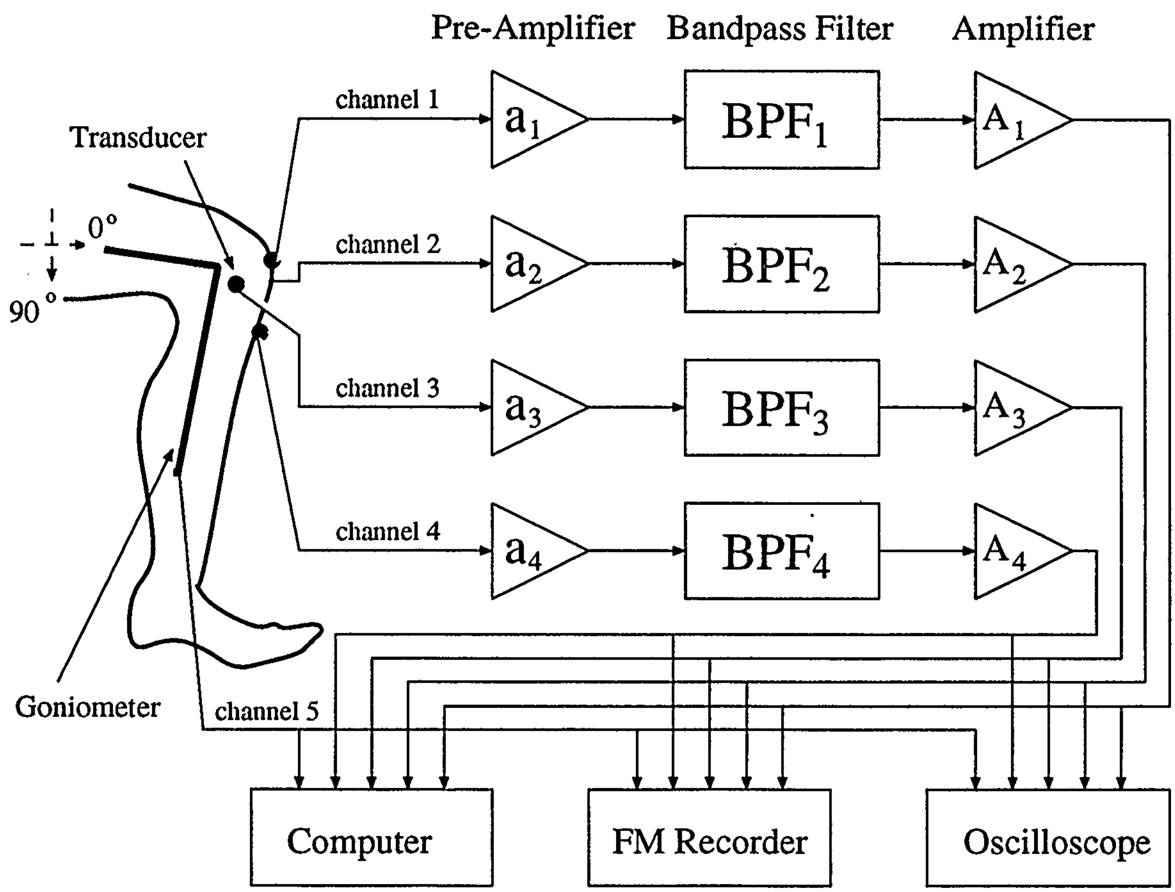

Figure 2.1 Multi-channel knee vibration detection and recording system. Channels 1 to 4 are used to record knee joint VAG signals (at MP - mid-patella, LC - lateral condyle, MC - medial condyle, and TT - tibial tuberosity), with Channel 5 recording the corresponding angle information. (Note: The transducer of Channel 2 not visible in this figure.)

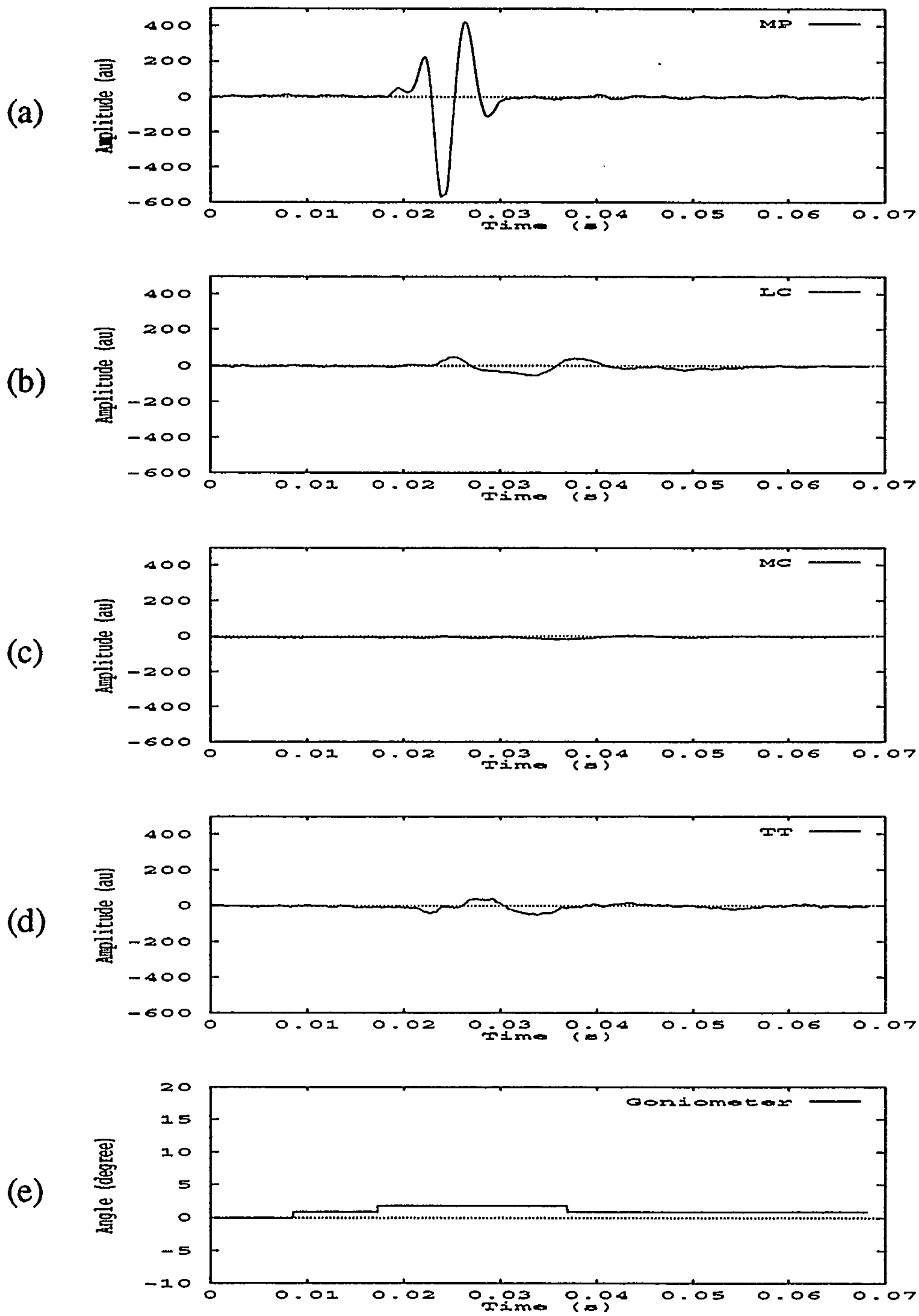

Figure 2.2 VAG signals of a normal subject in response to a tap over the upper-pole of the patella. (a) VAG signal at MP; (b) VAG signal at LC; (c) VAG signal at MC; (d) VAG signal at TT; (e) Joint angle. (*au*: Arbitrary units for acceleration; the accelerometer was not calibrated.)

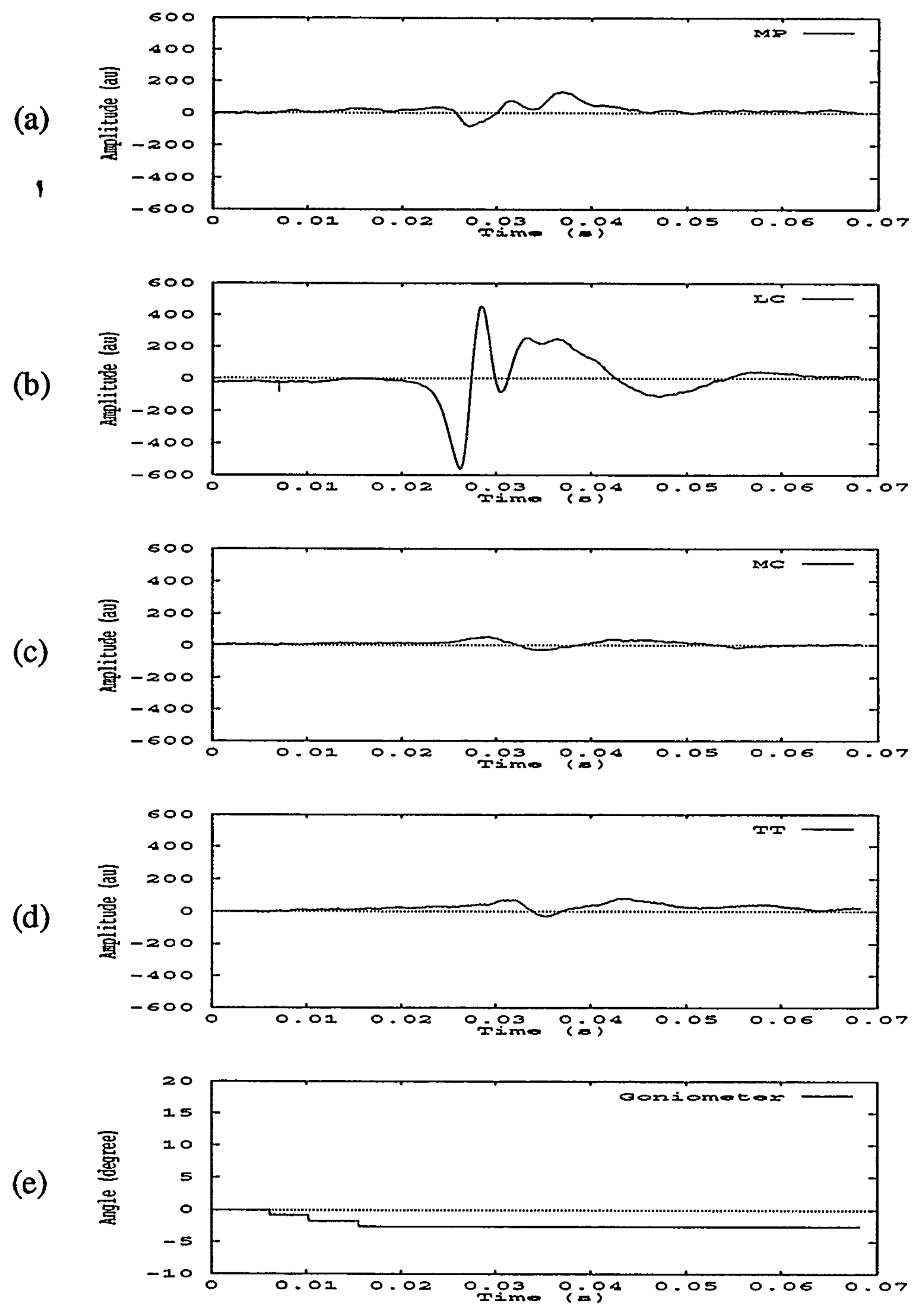

Figure 2.3 VAG signals during swinging movement of a patient with lateral chondromalacia and medial patella chondromalacia. (a) VAG signal at MP; (b) VAG signal at LC; (c) VAG signal at MC; (d) VAG signal at TT; (e) Angle during movement.

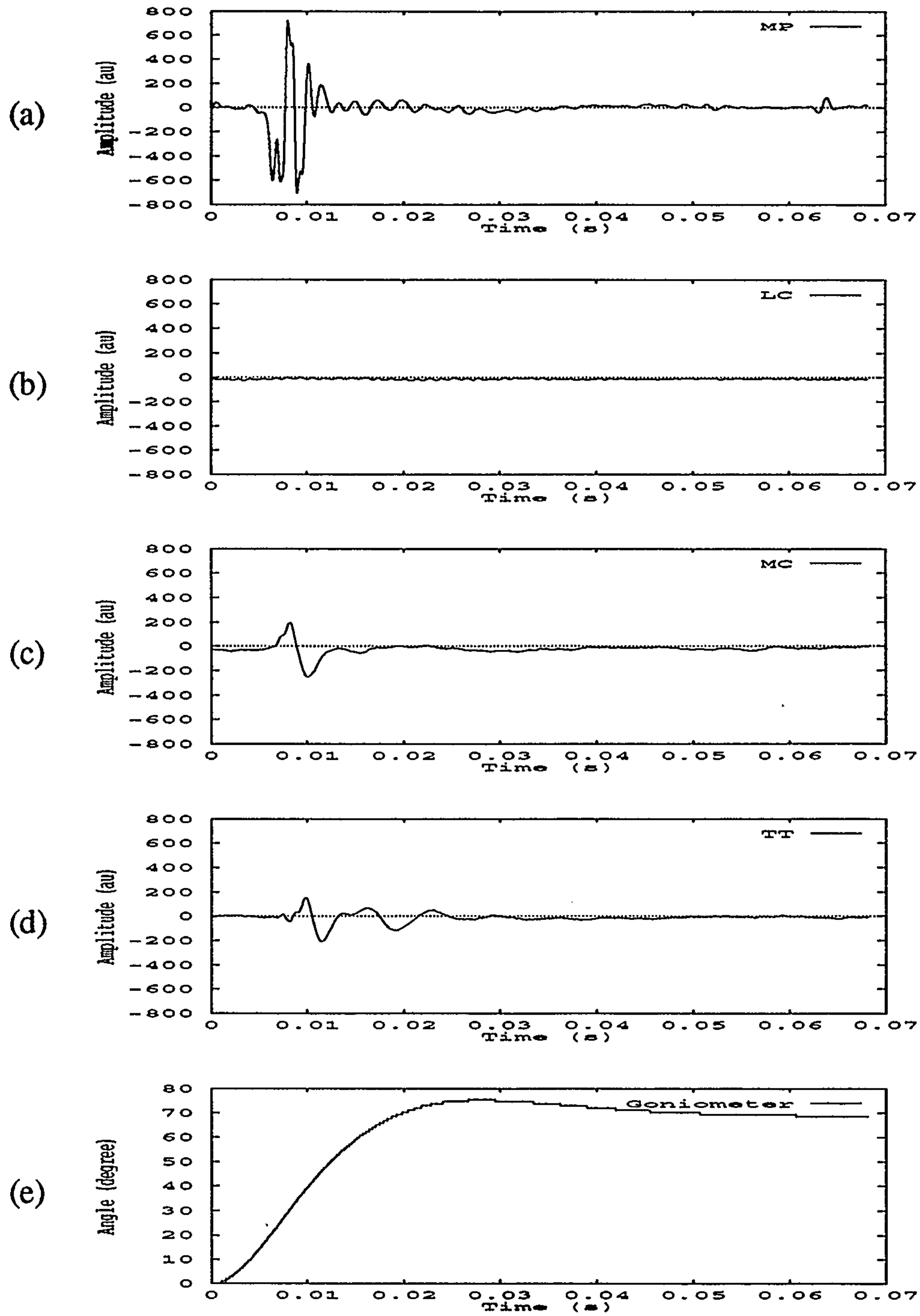

Figure 2.4 VAG signals during swinging movement of a cadaver knee with lesions near the mid-patella. (a) VAG signal at MP; (b) VAG signal at LC; (c) VAG signal at MC; (d) VAG signal at TT; (e) Angle during movement.

CHAPTER 3

TRANSFER FUNCTION ESTIMATION

3.1 Introduction

One might consider any signal analysis problem as consisting of some sort of a source, a transmission medium, and a receiver. The transmission medium could be an important and integral part of the whole system. In studying vibration or sound signals, it is advisable to begin with the generation, transmission, and reception of the signals.

3.2 Sound Transfer Characteristics

The sound source and transducer are coupled by a sound transmission path. This path may be through a simple homogeneous medium or through an inhomogeneous medium. It is clear that different media have different transmission characteristics.

3.2.1 Sound Transmission in General Media

In homogeneous media, such as air, water, or a solid brick wall, the transmission characteristics are simple because only transmitted waves are generated and the speed of sound does not change. When a sound wave travelling in one medium encounters the boundary of a second medium, transmitted waves as well as reflected waves are generated. Discussion of this phenomenon is greatly simplified if it is assumed that both the incident wave and the boundary between the media are planar and that all media are fluids. Complications arise when one of the media is a solid: the speed of sound in a solid, based on the bulk modulus, is different from that in a fluid [35]. The characteristic impedances of media and the angles of incidence and reflection are all factors that decide sound reflection and transmission [35].

The reflection of vibration or sound in a fluid from the surface of a solid and the transmission in the solid are somewhat more involved than any other case. No single simple method is available for analyzing the reflection or transmission of sound obliquely incident on the surface of a solid. Because of the differences in the porosity and internal elastic structure of various solids, the nature of the transmitted sound wave varies widely, and thereby influences the reflected sound wave. For instance, the sound wave transmitted into the solid may be refracted (1) so that it is propagated effectively only perpendicular to the surface, (2) in a manner similar to a plane wave entering a second fluid, or (3) into two waves: longitudinal bulk waves traveling in one direction and transverse shear waves traveling at a lower speed and in a different direction. These factors could affect the results of time delay estimation (to be discussed in chapters 4 and 6).

Another important factor associated with sound transmission characteristics is the vibrating body. Ideally, the vibrating body is rigid so that it could be considered as being concentrated at a single point. However, most cases are not as simple.

3.2.2 Sound Transmission in Human Tissues

Based on the description in the preceding section, sound transmission in the human body could be complicated because of its complex structure and the variety of tissues. Quantitative information as to the transmission and dissipation of vibratory energy in human body tissue is basic for the understanding of all mechanical phenomena occurring in the organism. Von Gierke studied the transmission of vibratory energy through human tissue [36]. He discussed the dynamic mechanical response of tissue exposed to vibrations, and pointed out that one can distinguish among three frequency ranges which exhibit different characteristics depending on the the ratio of tissue dimensions to wavelength. At very low frequencies below approximately 100 Hz, the body may be considered as a lumped parameter system. The tissue masses are coupled rather tightly by ligaments and muscles, and since they are elastically suspended in this way, resonance occurs; soft tissue serves as a damping medium. For higher frequencies, all through the audio frequency range and up to the order of magnitude of 100 kHz, wave propagation of vibration and mechanical impulses becomes more and more important; but the type of wave propagation found - shear waves, surface waves, or compressional waves - is largely determined by boundaries and geometric configurations. Above 100 kHz and to the MHz range, compression waves propagated and reflected in a beam-like manner through the medium predominate. The tissue dimensions are large compared to the wavelength in this range.

The velocity and absorption of high-frequency sound in mammalian tissues are described in a paper by Goldman and Hueter [37]. At high frequencies, the velocity of sound in an in vivo limb is about 1540 m/s (at 2.5 MHz), and 1476 m/s in refrigerated fat (at 1.8 MHz). The absorption of high-frequency sound is 0.1 cm^{-1} at 0.80 MHz frequency for refrigerated muscle, $1.5 - 4.5$ cm^{-1} in the range $0.8 - 0.6$ MHz for fresh or fixed skull bone, and $0.1 - 0.4$ cm^{-1} in the range $2.5 - 7.0$ MHz in fresh fat. They found that most measured velocities fall in the range from 1500 to 1600 m/s. Comparing the various soft tissues amongst each other, one notices that fat exhibits the lowest value of both sound velocity and absorption while muscle shows the highest values in both respects.

Clinical experience has well established certain areas on the thorax as being optimal for studying sounds from particular origins. In recent years there have been many efforts to analyze the transmission characteristics of various components of the body, with significant successes in studies of heart sounds and lung sounds.

3.2.2.1 Transmission Characteristics of Heart Sounds

Clinicians have long been aware of the transmission of heart sounds and murmurs from their cardiac source to various locations on the chest wall. Many researchers have studied the transmission paths of heart sounds and murmurs and the ability of the heart to transmit artificial mechanical vibration.

It was generally assumed that transmission of heart sounds and murmurs occurs through the blood mass within the heart and the great vessels. In the 1960s, Faber and Burton [38] studied the spread of heart sounds over chest wall and found that the spread velocity of heart sounds was from several m/s to a few tens of m/s, but under 100 m/s. Further, Faber [39] worked on the propagation of heart sounds in dogs by attaching several microphones to the chest wall and noting the time of arrival of the vibrations of the mitral component of the first heart sound at these locations. From the velocity of transmission, calculated by the arrival time of the vibrations at these listening sites, Faber concluded that transmission could not be by way of the blood mass, but rather through the ventricular wall. Heintzen and Vietor [40] applied a vibratory tone to the anterior chest wall and, using a phonocatheter, detected the portion of this vibration that reached the intracardiac blood mass. Their results clearly indicated a phasic variation in the chest wall to intracardiac blood transmissibility. In separate studies, Zalter et al. [41] and Feruglio [42] placed sound-generating catheters in the heart and studied the transmission of the resulting vibrations. However, no systolic-diastolic phasic variation was reported in these studies.

Systolic-diastolic phasic alteration of left ventricular mechanical vibration transmissibility was studied by Smith et al. [43]. They detected the percentage of the vibration that was transmitted from the source to the sensor by applying a continuous vibratory tone to the base of the heart in open-chest anesthetized dogs. They compared these data with those from intracardiac phonocardiograms obtained using a micromanometer-tipped catheter. It was found that in systole, the ventricle transmitted a vibratory tone from the cardiac base to the apex so that it was readily detected by the heart surface sensor. In contrast, the relaxed ventricle failed almost completely to transmit the vibration to the apical position during diastole. Eventually, the ventricular diastolic vibration transmissibility was found to equal or exceed that of the systolic phase when the dog experienced heart failure during hypoxia.

3.2.2.2 Transmission Characteristics of Lung Sounds

Another significant application of studies of vibration transmission in the human chest is the study of lung sounds. One of the earlier works on the acoustic transmission characteristics of the thorax is a report by Zalter and his group [41]. Three complementary avenues of approach were simultaneously undertaken by them in order to resolve qualitatively and quantitatively the transmission characteristics of the thoracic network. Their results showed that it is possible that different heart locations and suspension and different structures of the chest wall could cause some difference in the transmission of sounds in human beings. A transmission loss of $20 - 40\ dB$ was obtained for the various areas in the supine position. In the left lateral position, a transmission loss of $6\ dB$ was obtained for the second heart sound as transduced from the arterial roots. The first heart sound (apical), on the other hand, showed no transmission loss. Over the pulmonic area, a transmission loss of $8\ dB$ was obtained for the first sound as compared with the direct epicardial magnitude.

In 1986, Iyer et al. [44] studied the reduction of heart sounds from lung sounds by adaptive filtering. This technique was found to reduce the heart sounds by 50 to 80 percent. They discussed the application of autoregressive modeling to lung sound analysis in another paper [45]. They modeled the acoustic transmission through the lung parenchyma and chest wall as an all-pole filter and estimated the source and transmission characteristics of lung sounds separately based on the lung sounds at the chest wall. While analyzing an inspiratory segment of bronchial breath sounds, they showed that the sound is random white noise, and that the typical transmission filter frequency band is around $0 - 600$ Hz (central frequency around 400 Hz). The results for an inspiratory portion of vesicular breath sounds showed that the sound characteristics were indistinguishable from bronchial breath sounds, but that the typical transmission filter frequency response was smaller with a lower range ($0 - 300$ Hz, central frequency around 150 Hz). This difference was expected since vesicular sounds are known to have a longer transmission path with inertial components than the bronchial sounds, which leads to their getting filtered to a greater extent. For a segment containing an asthmatic expiratory wheeze, the estimated sound was found to be a periodic train of impulses and its spectrum was essentially white. The corresponding transmission filter frequency response was found to be lowpass, with a distinct resonance at 166 Hz. For an expiratory segment of vesicular lung sounds in early pneumonia, the transmission filter response shifted to higher frequency (central frequency around 250 Hz). In late pneumonia, an expiratory segment of lung sounds contained coarse crackles. The source waveform had impulsive bursts corresponding to the crackles and the transmission filter response was at a higher frequency (central frequency around 250 Hz). Therefore, there is significant correlation between the expected associated phenomena of diseases and the affected "source" and "transmission filter" characteristics of the computed model for lung sounds.

3.2.3 Sound Transmission in the Knee

The transmission of vibration signals through the knee joint is an important factor which may influence the frequency and intensity distribution of VAG signals recorded on the skin surface of the joint. The complex structure and mechanical system of the knee joint makes it difficult to estimate the transmission characteristics. The structure of the human knee is complicated, and consists of bone, cartilage, muscle, tendon, ligament, and fluids. This inhomogeneous characteristic of the knee results in complex transmission characteristics. It may not be appropriate to use simple acoustic transmission theory to detect or explain sound transmission in the human knee.

In natural VAG, the vibration sound energy is generated inside the knee and is recorded externally at the skin surface over the knee. The source could be at any position inside the knee joint, and the sounds could be transmitted in many paths. Aspects of transmission of VAG signals through joints remain unclear. This is probably due to the lack of proper devices for joint vibration measurement and the difficulty in performing such vibration measurements in a complex and inhomogeneous structure such as the knee joint.

There exist a few parameters which could aid in the analysis of sound transmission, such as attenuation, energy ratio of output and input signals, and time delays at different locations. In practice, the input signal is always unknown. Determination of the transfer function of the joint vibration system could have a significant impact on later development of the VAG technique as a non-invasive diagnostic tool for diagnosis of joint disorders.

3.3 Estimation of Transfer Functions

The transfer function for a constant-parameter, linear time-invariant system is the Laplace transform of the unit impulse response function that describes the system. Consider that a linear time-invariant system has the input $x(t)$ and the output $y(t)$. The system can be characterized by its impulse response $h(t)$ which is defined as the output when the input is the unit impulse function $\delta(t)$ and all the initial conditions are zero [46].

3.3.1 Transfer Functions of Single-Input Single-Output Systems

For a single-input single-output system, the transfer function $H(s)$ is defined as

$$H(s) = \mathcal{L}[h(t)] = \frac{Y(s)}{X(s)}, \tag{3.1}$$

where

$$X(s) = \mathcal{L}[x(t)], \tag{3.2}$$

and

$$Y(s) = \mathcal{L}[y(t)], \tag{3.3}$$

with $\mathcal{L}$ representing the Laplace transform, and with all the initial conditions set to zero.

Although the transfer function of a linear system is defined in terms of the impulse response, in practice, the input-output relation of a linear time-invariant system with continuous-data input is often described by a differential equation, so that it is more appropriate to derive a general-form transfer function directly from the differential equation. Then, the input-output relation of a linear time-invariant system is described by the following nth-order differential equation with constant real coefficients:

$$\frac{d^n y(t)}{dt^n} + a_n \frac{d^{n-1}y(t)}{dt^{n-1}} + \cdots + a_2 \frac{dy(t)}{dt} + a_1 y(t) =$$
$$b_{m+1}\frac{d^m x(t)}{dt^m} + b_m \frac{d^{m-1}x(t)}{dt^{m-1}} + \cdots + b_2 \frac{dx(t)}{dt} + b_1 x(t). \tag{3.4}$$

The coefficients $a_1, a_2, \cdots, a_n$ and $b_1, b_2, \cdots, b_{m+1}$ are real constants, and $n \geq m$. To obtain the transfer function of the linear system that is represented by Eq.3.4, we simply take the Laplace transform on both sides of the equation, and assume zero initial conditions. The result is

$$(s^n + a_n s^{n-1} + \cdots + a_2 s + a_1)Y(s) = (b_{m+1}s^m + b_m s^{m-1} + \cdots + b_2 s + b_1)X(s). \tag{3.5}$$

The transfer function between $x(t)$ and $y(t)$ is given by

$$H(s) = \frac{Y(s)}{X(s)} = \frac{b_{m+1}s^m + b_m s^{m-1} + \cdots + b_2 s + b_1}{s^n + a_n s_{n-1} + \cdots + a_2 s + a_1}. \tag{3.6}$$

In Eq.3.6, the transfer function is expressed only as a function of the complex variable s. It is not a function of the real variable, time, or any other variable that is used as the independent variable. When a system is subject to discrete-time or digital input, it may be more convenient to model the system by a difference equation; then, the transfer function becomes a function of the complex variable z (or ω), when the z-transform (or the Fourier transform) is used, which will be discussed in chapter 5.

3.3.2 Transfer Functions of Multivariable Systems

The definition of transfer function is easily extended to a system with multiple inputs and outputs, which is often referred to as a multivariable system. In general, if a linear system has p inputs and q outputs, the transfer function $H_{ij}(s)$ between the ith output $y_i(t)$ and the jth input $x_j(t)$ is defined as:

$$H_{ij}(s) = \frac{Y_i(s)}{X_j(s)}, \tag{3.7}$$

with $X_k(s) = 0$, for $k = 1, 2, \cdots, p$, $k \neq j$. The ith output transform of the system is related to all the input transforms by

$$\begin{aligned} Y_i(s) &= H_{i1}(s)X_1(s) + H_{i2}(s)X_2(s) + \cdots + H_{ip}(s)X_p(s) \\ &= \sum_{j=1}^{p} H_{ij}(s)X_j(s), \qquad (i = 1, 2, \ldots, q) \end{aligned} \tag{3.8}$$

where $H_{ij}(s)$ is defined in Eq.3.7. It is convenient to represent Eq.3.8 by the matrix equation

$$\boldsymbol{Y}(s) = \boldsymbol{H}(s)\boldsymbol{X}(s), \tag{3.9}$$

where

$$\boldsymbol{Y}(s) = \begin{bmatrix} Y_1(s) \\ Y_2(s) \\ \vdots \\ Y_q(s) \end{bmatrix} \tag{3.10}$$

is a $q \times 1$ matrix, called the transformed output vector; and

$$\boldsymbol{X}(s) = \begin{bmatrix} X_1(s) \\ X_2(s) \\ \vdots \\ X_p(s) \end{bmatrix} \tag{3.11}$$

is a $p \times 1$ matrix, called the transformed input vector;

$$\boldsymbol{H}(s) = \begin{bmatrix} H_{11}(s) & H_{12}(s) & \cdots & H_{1p}(s) \\ H_{21}(s) & H_{22}(s) & \cdots & H_{2p}(s) \\ \vdots & \vdots & \vdots & \vdots \\ H_{q1}(s) & H_{q2}(s) & \cdots & H_{qp}(s) \end{bmatrix} \tag{3.12}$$

is a $q \times p$ matrix, called the transfer function matrix.

3.4 Applications of Transfer Functions

The theory of transfer function has been applied in a variety of areas, such as communication, power, control, and signal analysis. It is known to be used in industry widely. Many applications in biomedical engineering have also been reported.

The influence of cardiac action on the transfer function of the heart-thorax acoustic system was studied by Feruglio [42] and Heintzen and Vietor [40]. Their studies provided mainly qualitative information, and the role of cardiac action on the transfer function of the heart-thorax acoustic system remained unclear. In the 1980's, Durand and his group [47] developed a computer model capable of reflecting the dynamic behavior of the heart-thorax acoustic system to investigate this matter. The results of their studies showed that the transfer function of the heart-thorax acoustic system changes during the cardiac cycle. For the seven animals studied, it would appear that the contribution of left ventricular first and second sounds to the apical phonocardiogram is significant for frequencies below 70 Hz and negligible for frequencies above 250 Hz. In addition, it was shown that 80 percent of the power of sounds recorded on the chest wall arises from linear transmission of sounds recorded within the left ventricle through the heart-thorax acoustic system. The other 20 percent was explained as being due to thoracic noise, incoherent cardiac contributions, and the nonlinearity of the acoustic system.

In human knee joints, different pathologies may be expected to be associated with different transfer functions. The study of transfer functions or frequency response functions of knee VAG signals could aid diagnosis of various diseases in human knee joints. The application of transfer function analysis to the knee joint will be described in chapter 5.

CHAPTER 4

SOURCE LOCALIZATION AND TIME DELAY ESTIMATION

4.1 Introduction

Recently, many signal processing techniques have been proposed for source localization, and the techniques have been applied in various areas, such as machine component diagnosis, environmental noise measurement, and communication. The objective of this chapter is to describe some general methods for sound source localization and to discuss their associated applications.

4.2 Methods for Source Localization

There are two major methods of signal processing for source localization: coherence and time delay estimation. The coherence method could be divided into two parts: using magnitude and using phase. Time delay estimation involves more techniques, such as cross-correlation and adaptive estimation. Active and passive sonar or radar systems for localization could be also categorized as time delay estimation methods.

This section focuses on the basic theory of signal processing methods for sound source localization. It is divided into two parts: one treats coherence, and the other time delay methods.

4.2.1 Coherence

The coherence function is a measure of the accuracy of the assumed linear input/output model, and can also be computed from the measured autospectral and cross-spectral density functions. Before the representation of coherence function is given, some involved functions are described here. For a pair of stationary random processes $x(t)$ and $y(t)$, the covariance functions are independent of t.

For arbitrary fixed t and τ, define

$$R_{xx}(\tau) = E[x(t)x(t+\tau)], \tag{4.1}$$

$$R_{yy}(\tau) = E[y(t)y(t+\tau)], \tag{4.2}$$

$$R_{xy}(\tau) = E[x(t)y(t+\tau)]. \tag{4.3}$$

where $E[\cdot]$ represents the statistical expectation operator. The quantities $R_{xx}(\tau)$ and $R_{yy}(\tau)$ are called the autocorrelation functions of $x(t)$ and $y(t)$, respectively, whereas $R_{xy}(\tau)$ is called the cross-correlation function between $x(t)$ and $y(t)$ for the specified time difference or delay τ.

The Fourier transforms of the correlation functions are defined by

$$S_{xx}(f) = \int_{-\infty}^{\infty} R_{xx}(\tau)e^{-j2\pi f\tau}d\tau, \tag{4.4}$$

$$S_{yy}(f) = \int_{-\infty}^{\infty} R_{yy}(\tau)e^{-j2\pi f\tau}d\tau, \tag{4.5}$$

$$S_{xy}(f) = \int_{-\infty}^{\infty} R_{xy}(\tau)e^{-j2\pi f\tau}d\tau. \tag{4.6}$$

The quantities $S_{xx}(f)$ and $S_{yy}(f)$ are called the autospectral density functions of $x(t)$ and $y(t)$, respectively, whereas $S_{xy}(f)$ is called the cross-spectral density function between $x(t)$ and $y(t)$.

The one-sided autospectral density functions, $G_{xx}(f)$ and $G_{yy}(f)$, where f varies only over $[0, \infty)$, are defined by

$$G_{xx}(f) = \begin{cases} 2S_{xx}(f) & 0 \le f < \infty \\ 0 & otherwise \end{cases}, \tag{4.7}$$

$$G_{yy}(f) = \begin{cases} 2S_{yy}(f) & 0 \le f < \infty \\ 0 & otherwise \end{cases}. \tag{4.8}$$

The one-sided cross-spectral density function $G_{xy}(f)$, where f varies only over $[0, \infty)$, is defined by

$$G_{xy}(f) = \begin{cases} 2S_{xy}(f) & 0 \leq f < \infty \\ 0 & otherwise \end{cases} . \tag{4.9}$$

$G_{xy}(f)$ may also be presented in complex polar notation as

$$G_{xy}(f) = |G_{xy}(f)|e^{-j\theta_{xy}(f)} \qquad 0 \leq f < \infty, \tag{4.10}$$

where $\theta_{xy}(f)$ is the phase of the cross-spectral density function. The coherence function (sometimes called the coherency squared function) may now be defined by

$$\gamma_{xy}^2(f) = \frac{|G_{xy}(f)|^2}{G_{xx}(f)G_{yy}(f)} = \frac{|S_{xy}(f)|^2}{S_{xx}(f)S_{yy}(f)} \tag{4.11}$$

and satisfies for all f,

$$0 \leq \gamma_{xy}^2(f) \leq 1. \tag{4.12}$$

Clearly, $\gamma_{xy}^2(f) = 1$ for a single-input, single-output linear system at all frequencies. If there is another uncorrelated signal source adding to the output $y(t)$, such as a signal $z(t)$, then the measured coherence will be less than 100%. Thus, coherence is a way of expressing dependence through comparison. With coherence, multi-path problems can be investigated since $\gamma_{xy}^2(f)$ measures the amplitude effects of all sound energy reaching the sensor by many paths. The dominant sound source could be detected by analyzing coherence.

4.2.2 Time Delay

Rapid developments in time delay estimation (TDE) theory have been made in recent years. Many different methods for TDE are based on cross-correlation analysis.

4.2.2.1 Cross-correlation

Correlation techniques have been used extensively in various scientific and technological fields for a number of years. Time delay analysis is a common application of correlation techniques. Consider two sensors at different locations which register the signal emanating from a source. The correlated signals are assumed to be band-limited, stationary, Gaussian processes corrupted by non-cross-correlating noise. The position of the peak in an observed cross-correlation curve is interpreted as the time delay estimate.

The typical method based on cross-correlation is the general cross-correlation method (GCC). The model of the GCC technique is shown in Fig. 4.1. A signal emanating from a remote source and monitored in the presence of noise at two spatially-separated sensors can be mathematically modeled as

$$x_1(t) = s_1(t) + n_1(t), \tag{4.13}$$

$$x_2(t) = \alpha s_1(t + D) + n_2(t), \tag{4.14}$$

where $s_1(t)$, $n_1(t)$, and $n_2(t)$ are real, jointly-stationary random processes, α is an attenuation factor, and D is the time delay between the two paths. The signal $s_1(t)$ is assumed to be uncorrelated with the noise processes $n_1(t)$ and $n_2(t)$.

The cross-correlation function between $x_1(t)$ and $x_2(t)$ is given by [48]

$$R_{x_1x_2}(\tau) = E[x_1(t)x_2(t-\tau)]. \tag{4.15}$$

Given a finite observation time T, $R_{x_1x_2}$ can be estimated as

$$\hat{R}_{x_1x_2}(\tau) = \frac{1}{T-\tau}\int_{\tau}^{T} x_1(t)x_2(t-\tau)dt. \tag{4.16}$$

In order to improve the accuracy of the delay estimate $\hat{D}$, it is desirable to prefilter $x_1(t)$ and $x_2(t)$ prior to the integration. As shown in Fig. 4.1, x_i may be filtered through H_i to yield y_i for $i = 1, 2$. The resultant y_i are multiplied, integrated, and squared for a range of time shifts, τ, until the peak is obtained. The time shift causing the peak is an estimate $\hat{D}$ of the true delay D.

The cross-correlation between $x_1(t)$ and $x_2(t)$ is related to the cross-power-spectral density function $G_{x_1x_2}(f)$ by the well-known Fourier transform relationship [48]

$$R_{x_1x_2}(\tau) = \int_{-\infty}^{\infty} G_{x_1x_2}(f)e^{j2\pi f\tau}df. \tag{4.17}$$

When $x_1(t)$ and $x_2(t)$ have been filtered as depicted in Fig. 4.1, the cross-power-spectrum between the filter outputs is given by [48]

$$G_{y_1y_2}(f) = H_1(f)H_2^*(f)G_{x_1x_2}(f), \tag{4.18}$$

where * denotes the complex conjugate. Therefore, the generalized correlation between $y_1(t)$ and $y_2(t)$ is [48]

$$R_{y_1y_2}^{(g)}(\tau) = \int_{-\infty}^{\infty} \Psi_g(f)G_{x_1x_2}(f)e^{j2\pi f\tau}df, \tag{4.19}$$

where

$$\Psi_g(f) = H_1(f)H_2^*(f) \tag{4.20}$$

denotes the general frequency weighting.

4.2.2.2 Bearing and Range Estimation

Another method for source localization is bearing and range estimation. The fundamental physical problem of time delay analysis can be described as follows. There are two receiving sensors, which receive waveforms $x_1(t)$ and $x_2(t)$. An attempt is made to determine the bearing of the source by estimating the time delay between the received signals. Essentially, there is a signal with noise, and a delayed signal with noise:

$$x_1(t) = s(t) + n_1(t), \tag{4.21}$$

$$x_2(t) = s(t-D) + n_2(t). \tag{4.22}$$

In the ideal case, or at least to make the problem mathematically tractable, we assume the noise sources are uncorrelated with each other and also with the source signal. We also assume that the signals and noise are stationary Gaussian random processes, and that the observation time is large compared to the delay D.

If there were three sensors instead of two, the first two sensors could provide one time delay bearing estimate, and the other two could provide another time delay bearing estimate. The point at which these bearings intersect would yield an estimate of the source location in both range and bearing.

A. Active System

To measure the range of a source (or target) in an active system, it is necessary to estimate the time delay D at which the echo arrives at the receiver. If the time from the transmission of the pulse is measured, the range of the target is $PD/2$, where P is the speed of sound or electromagnetic wave. The received signal will consist of a deterministic signal that is corrupted with white noise of spectral density. Then, the standard deviation of time delay errors about the true time delay is given by [49]

$$\sigma_D = \left(\frac{1}{8\pi^2}\right)^{1/2} \frac{1}{\sqrt{SNR}} \frac{1}{\sqrt{TW}} \frac{1}{f_0} \frac{1}{\sqrt{1 + W^2/12f_0^2}} \tag{4.23}$$

where T is the observation time, SNR is the signal-to-noise ratio, W is the bandwidth, and f_0 is the center frequency of the band. Eq. 4.23 shows that σ_D is inversely proportional to: 1) the square root of the SNR; 2) the square root of the product of bandwidth and time; 3) the center frequency of the band and that it is also a function of the of bandwidth and center frequency of the band.

B. Passive System

In a passive system, the received signals are composed of the signals generated by the source (or target) and noise. It is assumed that the source signal and noise are not correlated and that they are stationary random processes. The expression for standard deviation of time delay about the true time delay is similar to Eq.4.23 [49] except that the term with $\sqrt{SNR}$ is replaced by SNR at low SNR. At high SNR, the standard deviation of the time delay estimate varies inverserly as the square root of the SNR, and the effects of the other parameters such as T and W remain the same.

The effectiveness of the method for time delay estimation could be implied from the standard deviation of the time delay estimation. However, an investigation of the usefulness of the standard deviation in predicting the performance of bearing and range estimation is deemed advisable [49].

4.2.2.3 Adaptive Time Delay Estimation

The adaptive method is a common method to track and estimate the time delay in a signal between two sensors. The least-mean-square (LMS) adaptive filter was applied to determine the time delay in a signal between two split-array outputs [50, 51]. A recursive LMS algorithm and a peak detection algorithm have also been suggested for adaptive time delay estimation [52].

The system model used in the development of the adaptive delay element for time delay estimation is given in Fig. 4.2 [53]. One channel contains the signal s_m, m being the time index or sample number, and the other channel contains the signal s_{m-D}, a delayed version of s_m. In order to drive the error to a minimum, the variable delay d is modified until it "locks" onto a value that minimizes the error e_m. This value of the variable delay is then the estimate of the time delay between the two signals. The optimal delay is obtained by using a recursive algorithm for modifying the continuous delay $\hat{d_m}$ [53]:

$$\hat{d}_{m+1} = \hat{d}_m + \mu e_m (s_{m-d-1} - s_{m-d+1}) \tag{4.24}$$

where μ is a convergence parameter ($\mu > 0$), and $e_m = s_{m-D} - s_{m-d}$.

4.3 Applications of Source Localization

The theories and models of most methods of source localization have been described above. Each one of the aforementioned techniques has certain advantages and limitations depending upon the nature of the signal and noise sources. This section will discuss some applications associated with these methods.

4.3.1 Environmental Applications

The methods of coherence and cross-correlation are the major techniques used for localization of environmental noise. Although the theory of coherence has been well established, modern digital Fourier transform processors which reduce the measurement of coherence to a push-button operation have only recently become available. But the technique is relatively new, and only a few applications of coherence to noise source identification have been described in the literature to date. Roth [54] measured the coherence between an accelerometer on a fan-transformer case and a far-field microphone. Eberhardt and Reiter [55] have used the same technique to compare the vibration of a truck tire with the radiated sound. When the noise source is clearly radiating discrete frequency components, a near-field to far-field coherence measurement will yield information on the individual noise source spectra. A two-microphone measurement system for the detection of car exhaust noise in the presence of engine noise has been described by Ishii and Ishida [56]. They assumed that the microphone placed at the rear of the car measured predominantly the near-field exhaust pressures, so the multiplication of the far-field spectrum by the coherence function predicted that part of the noise radiated by the exhaust.

A test for the location of the major noise radiating areas is to measure the multiple coherence for the multiple input system case. It can be shown [57] that the power spectral density of the output is related to the inputs by

$$G_y(f) = \sum_{i=1}^{N} \sum_{j=1}^{N} H_i^*(f) H_j(f) G_{ij}(f), \tag{4.25}$$

where N is the number of inputs. The cross-spectrál density, $G_{iy}(f)$, between the output $y(t)$ and the ith input $x_i(t)$ is given by

$$G_{iy}(f) = \sum_{j=1}^{N} H_j(f) G_{ij}(f). \tag{4.26}$$

The partial coherence function for noise source detection, which is perhaps the most notable contribution to coherence techniques, was used to investigate the noise generating mechanisms of a punch-press [58]. Coherence is a useful quantity, but is difficult to estimate. The more common methods applied in source localization use time delay measurements.

Time delay estimation (TDE) is often referred to by other names, including time delay (TD), time difference of arrival (TDOA), group delay, time-of-arrival difference (TOAD), delay, delay time, and phase delay. These terms often have the same meaning. TDE has been widely used in environmental noise localization.

The estimation of time delays between signals received at two or more sensors is an important issue in active and passive signal processing, communication and radar or sonar systems, and in other fields. Numerous techniques have been proposed to estimate the time delay and some of its variations. Most of the techniques proposed for time delay estimation are based on the generalized correlation method.

As early as 1954, Goff [59] used cross-correlation techniques to detect dominant sources of noise in a machine shop. He was able to use measurements of cross-correlation to ascertain the noisiest machines in a workspace containing up to nine machines. Since cross-correlation provides an overall comparison of the amplitudes of two signals at every frequency as well as a measure of the mean time (phase) difference between them, it follows that the path-time of transmission of the sound between the noise source and the far-field microphone is the key to the location of the noise source. This path-time is obtained by determining the time delay which maximizes the cross-correlation coefficient. Siddon [60] used this technique to find the exact location of the noise source produced by the aerodynamic swirling motion in an automobile tire. A further example of the use of the time delay measurement as a geometrical technique for pinpointing the source position has been given by Pease [61], who used this technique to detect jet noise.

4.3.2 Passive Sonar

A major application of sound localization is range and bearing estimation for passive sonar. The sonar target to be passively localized is a source of wide-band zero-mean Gaussian noise, and the range from the array to the source is large enough so that the amplitude gradient of the noisy signal across the array is negligible. Hahn [62] reported on optimum signal processing for passive sonar range and bearing estimation. The Cramér-Rao matrix bound (CRMB) was used to determine an optimum signal processor. The optimum processor was configured as a set of $M(M-1)/2$ cross-correlator delay estimators (one for each hydrophone pair; M is the number of the sensors), followed by a Gauss-Markov estimation of the array delay vector (target steering vector), which in turn was followed by a linear weighting of the estimated delay vector elements to determine a bearing estimate and a range estimate. The results of his study showed that the estimation of range and bearing can be done so that the error covariance matrix is the CRMB; no better estimates for range and bearing exist.

Carter [63] studied time delay estimation for passive sonar signal processing. An overview of applied research in passive sonar signal processing estimation techniques for naval systems is presented in his paper. The source-state estimation problem is discussed in terms of estimating the position and velocity of a moving acoustic source. Optimum bearing and range estimation methods are presented for the planar problem and related to the optimum time delay vector estimator. Suboptimal realizations are considered together with the effects of source motion and receiver positional uncertainty in his paper.

Passive bearing can also be used to estimate a broad-band source, as proposed by Joseph [64]. The statistical mean on the bearing estimation problem is derived and the resulting bias defined in his paper.

Azizul [49] reported on time delay estimation in active and passive systems for target localization. He pointed out that sonar and radar systems not only detect targets but also localize them, and that the process of localization involves bearing and range estimation. These objectives of bearing and range estimation can be accomplished actively or passively, depending on the situation.

4.3.3 Communications

A new application of source localization in communications was reported by Gardner and Chen [65]. They applied signal-selective, time-difference-of-arrival estimation for passive localization of man-made signal sources in a highly corruptive environment. In their paper, a new class of passive source localization methods that exploit an inherent signal property is presented. The inherent property is characteristic of man-made signals used for communications and telemetry to obtain substantial tolerance to all types of interference and noise. These new methods cross-correlated frequency-shifted as well as time-shifted versions of the received data in order to exploit the unique property based on cross-correlation of time-shifted measurements of data from multiple receivers. Their results showed the bias in time delay estimates was only 10% and the standard deviation was about 10% to 20%.

4.3.4 Localization of Sound Sources in the Human Body

As mentioned above, various techniques could be used to estimate time delay or evaluate the standard deviation between the estimated time delay and the true time delay. Not each technique is suitable to estimate time delay to localize sources in the human body due to the characteristics of the signals and the sources. Bearing and range estimation is always used to localize sources in large areas, for example, target detection in the ocean. The coherence method is suitable to distinguish the contribution of multiple sources for which frequency distribution are known.

The main technique in heart sound localization is to obtain time delays at various recording sites by correlation and spectrum comparison measures [66, 48]. The locations of the sources could be computed by knowing these delays, the transducer positions, and a model for transmission of sound through the throax. In a study on the spread of heart sounds over the chest wall [38], multi-site phonocardiogram (PCG) signals were analyzed to measure actual time delays in the arrival of different heart sound components at different locations on the chest surface. The time differences between signal components were measured from photographic negatives of oscilloscope traces, and knowing the locations of the detectors, graphical methods were used to locate "secondary sources" on the chest surface. These source locations matched with the corresponding auscultatory areas. The apparent velocity of vibrational transmission of heart sounds was estimated in this study to be in the range from several m/s to a few tens of m/s. It was suggested that the sounds travel through the viscoelastic thoracic medium as transverse shear waves [38].

Although many techniques have been developed to analyze VAG signals in the human knee joint for removal of interference, signal segmentation, and classification, these techniques are unable to localize sound sources. Studies on multi-channel VAG signal analysis for source localization were commenced in 1992 at The University of Calgary [67].

The major purpose of the study for this thesis is source localization of human knee sounds or VAG signal components. The case of isolated sources in the human knee joint has been considered in this initial study. A model for knee sound source localization and its theory, algorithms, and applications will be discussed in chapter 6.

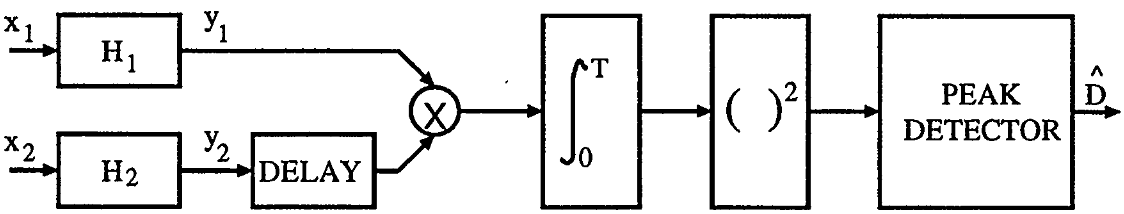

Figure 4.1 Model of the generalized cross-correlation method for estimation of time delay.

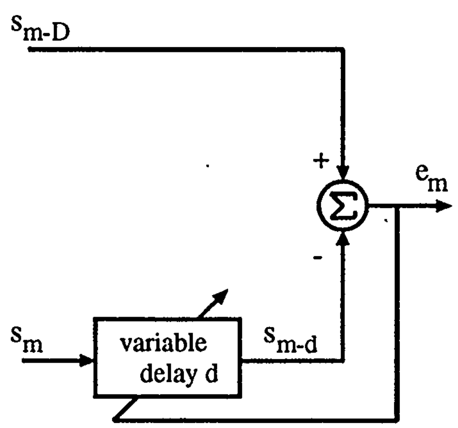

Figure 4.2 Model of the adaptive time delay estimation system.

CHAPTER 5

MODELING OF THE VIBROARTHROGRAPHIC FREQUENCY RESPONSE FUNCTION OF THE KNEE JOINT SYSTEM

5.1 Introduction

The knee joint is a complex mechanical system, the behavior of which could be altered by cartilage degeneration and meniscus damage [68]. VAG signals could provide information on the structural and functional integrity of the knee joint system [68, 69, 19, 24]. However, aspects of the transmission of VAG signals through joints remain unclear. In particular, the frequency response function, a special case of the transfer function, which describes transmission properties of the knee joint system, is not well documented. This is probably due to the lack of proper devices for joint vibration measurements and the difficulty in performing such vibration measurements in a complex and inhomogeneous structure such as the knee joint.

The transmission of vibration signals through the joint is an important factor which may influence the frequency and intensity distribution of VAG signals recorded on the skin surface of the joint. The determination of the frequency response function of the joint vibration system could have a significant impact on later development of the VAG technique as a non-invasive diagnostic tool for diagnosis of joint disorders [70]. The study with externally applied mechanical stimulation, as described in this chapter, represents the first step towards understanding and determination of the transmission properties of VAG signals. This chapter reports our experimental work carried out on normal, abnormal, and cadaver human joints. The intent is to determine the frequency response function of an equivalent knee joint system using the power density spectra of VAG signals simultaneously recorded over various positions of the joint. The initial findings reported here should provide insight into the estimation of the frequency response function and some implications with regard to the transmission characteristics of intrinsic knee sounds or VAG signals.

5.2 A Basic Model for Estimating the Frequency Response Function

A schematic representation of the basic model of the knee joint frequency response analysis system is shown in Fig. 5.1. The signal $s(t)$, representing the input signal of the model, is the VAG signal recorded from the position MP close to the site of mechanical stimulation. The signal $y_i(t)$ denotes the contribution of the MP signal to the signal at position i ($i = 1, 2, 3$, where "1" represents the position LC, "2" MC, and "3" TT), and $H_{pi}(f)$ denotes the frequency response function of the system between MP and the position i, which describes the vibrational properties of the joint structures. The additive noise $n_i(t)$ ($i = 1, 2, 3$) represents vibrational activities which are uncorrelated with the VAG signals. These noise components include ambient interference and any incoherent musculo-skeletal vibration contribution. The signal $v_i(t)$, at the model output, is the VAG signal recorded at the position i ($i = 1, 2, 3$). With this model, it is possible to describe the vibration transmission characteristics of the knee joint system by using classical system theory [71].

5.2.1 Estimation of the Frequency Response Function

In this study, the test is performed on the knee joint with the joint angle fixed at a specific value. The VAG signal is considered as a sample of a stationary process. Thus, in the basic model of the knee joint system, the auto-spectral density function of the input signal $s(t)$ can be computed by taking the Fourier transform of its auto-correlation function $R_{ss}(m)$, i.e.,

$$\hat{G}_{ss}(f) = \sum_{m=0}^{M-1} R_{ss}(m) e^{-j2\pi mf}, \tag{5.1}$$

and similarly the cross-spectral density function between the two VAG signals $s(t)$ and $v_i(t)$ can be estimated by

$$\hat{G}_{sv_i}(f) = \sum_{m=0}^{M-1} R_{sv_i}(m) e^{-j2\pi mf} \qquad i = 1, 2, 3, \tag{5.2}$$

where $R_{sv_i}(m)$ are the cross-correlation functions of the VAG signals $s(t)$ and $v_i(t)$. For the system represented by the model, the output spectrum at position i ($i = 1, 2, 3$) contributed by the input signal passing through $\hat{H}_{pi}(f)$ is called the coherent output spectrum, and is given by

$$\hat{G}_{y_i y_i}(f) = |\hat{H}_{pi}(f)|^2 \hat{G}_{ss}(f) \qquad i = 1, 2, 3, \tag{5.3}$$

and the total auto-spectrum of the signal at position i ($i = 1, 2, 3$) is the sum of the coherent output spectrum $\hat{G}_{y_i y_i}(f)$ and the noise spectrum $\hat{G}_{n_i n_i}(f)$, that is,

$$\hat{G}_{v_i v_i}(f) = \hat{G}_{y_i y_i}(f) + \hat{G}_{n_i n_i}(f) \qquad i = 1, 2, 3. \tag{5.4}$$

Eq.5.3 shows that the coherent output spectral density function can be determined from the input spectral density function and system magnitude response, or that the system magnitude response can be determined from the input and coherent output spectral density functions. The complete frequency response function of the system can also be determined from the cross-spectral density and auto-spectral density functions. With uncorrelated noise $n_i(t)$, the complete frequency response function $\hat{H}_{pi}(f)$ of the system representing the situation at a specific joint angle, can be estimated by [71]

$$\hat{H}_{pi}(f) = \hat{G}_{sv_i}(f) / \hat{G}_{ss}(f) \qquad i = 1, 2, 3. \tag{5.5}$$

5.3 Experiments on the Human Knee Joint

5.3.1 Mechanical Stimulation and Data Acquisition

Mechanical stimulation was performed on 14 adult subjects (10 patients with cartilage pathology, 2 normal subjects, and 2 cadavers) with a single finger tap over the upper-pole of the patella. VAG signals produced by the stimulation were obtained using the multi-channel vibration recording system described in Chapter 2, with four miniature accelerometers (Dytran 3115a) stuck onto the skin surface using two-sided adhesive tape at four positions: mid-patella (MP), lateral condyle (LC), medial condyle (MC), and tibial tuberosity (TT). The knee joint and hip angles were fixed at 90 degrees. The signals were amplified and filtered with a bandwith 10 Hz - 1 kHz and recorded. The bandwidth 10 Hz - 1 kHz was used to reduce noise due to the measurement system, cable swing, etc. It also serves for preventing the aliasing effects induced by digitization. The recorded signals were then digitized with a sampling rate of 15 kHz and 12 bits/sample.

5.3.2 Data Processing

Mean values different from zero should be removed from raw VAG data to obtain reliable estimates of the frequency response functuion. The first quantities to compute are thus the sample mean values

$$\bar{v}_m = \frac{1}{N}\sum_{i=0}^{N-1} v_m(i), \tag{5.6}$$

where N is the length of the data segment used (1024 samples in this work), v_m, $m = 1,2,3,4$, are the VAG signal segments, and $\bar{v}_m$ represents the mean of $v_m(i)$. Then,

$$x_m(i) = v_m(i) - \bar{v}_m; \quad m = 1,2,3,4; \quad i = 0,1,...,N-1, \tag{5.7}$$

correspond to the new VAG records with zero mean.

The following steps were used to compute the frequency response function [71] (assuming $x_1(n)$ and $x_2(n)$ to be the signals being analyzed):

1. Store $x_1(n)$ in the real part and $x_2(n)$ in the imaginary part of $z(n) = x_1(n) + jx_2(n)$, $n = 0, 1, ..., N-1$.

2. Augment both the real and imaginary parts with N zeros to obtain a new $z(n)$ sequence with $2N$ terms.

3. Compute the $2N$-point FFT giving $Z(k)$ for $k = 0, 1, ..., 2N-1$, as

$$Z(k) = \sum_{n=0}^{2N-1} [x_1(n) + jx_2(n)] e^{-j2\pi kn/2N}; \quad k = 0, 1, 2, ..., 2N-1. \tag{5.8}$$

4. Compute $X_1(k)$ and $X_2(k)$ for $k = 0, 1, ..., 2N-1$, using the following equations:

$$X_1(k) = \begin{cases} \Re e\{Z(0)\} & k = 0 \\ \dfrac{Z(k) + Z^*(2N-k)}{2} & k = 1, 2, \ldots, 2N-1 \end{cases} \tag{5.9}$$

$$X_2(k) = \begin{cases} \Im m\{Z(0)\} & k = 0 \\ \dfrac{Z(k) - Z^*(2N-k)}{2} & k = 1, 2, \ldots, 2N-1 \end{cases} \tag{5.10}$$

where * represents complex conjugation.

5. Compute the auto-spectral density function using

$$|G_{x_1x_1}(k)| = \frac{T_s}{2N} |X_1(k)|^2 \quad k = 0, 1, 2, ..., 2N-1, \tag{5.11}$$

$$|G_{x_2x_2}(k)| = \frac{T_s}{2N} |X_2(k)|^2 \quad k = 0, 1, 2, ..., 2N-1, \tag{5.12}$$

where T_s is the sampling interval, equal to $\frac{1}{15000}$ second in this work.

6. Compute the cross-spectral density function using

$$G_{x_1x_2}(k) = \frac{T_s}{2N}X_1^*(k)X_2(k) \quad k = 0, 1, 2, ..., 2N-1. \tag{5.13}$$

7. The frequency response function is obtained as the cross-spectral density function divided by the auto-spectral density function of the input signal.

The above procedure was repeated for every possible pair from the set of four signals recorded.

5.4 Results

5.4.1 In Vivo VAG Signals

Fig. 5.2 shows the averaged input and output spectral density functions and standard error of VAG signals of ten patients at various positions. As shown in Fig. 5.2(a), the auto-spectral density function of the VAG signal at the stimulation site (MP) has a peak at 80 Hz and a bandwidth of approximately 20 Hz to 215 Hz. The auto-spectral density function of the VAG signal at the LC position is given in Fig. 5.2(b), which has a peak at 50 Hz and a bandwidth of approximately 25 Hz to 85 Hz. Fig. 5.2(c) shows that the auto-spectral density function at the position MC has a peak frequency at 45 Hz and a bandwidth of approximately 30 Hz to 120 Hz. The corresponding auto-spectral density function at the position TT is shown in Fig. 5.2(d), which has a peak frequency of about 37 Hz and a bandwidth of approximately 20 Hz to 110 Hz. Above and below their peak frequency locations, the density functions decrease nonuniformly and reach values of about 90% of the maximum at 70 Hz and 90 Hz (MP); at 45 Hz and 52 Hz (LC); at 43 Hz and 46 Hz (MC); and at 30 Hz and 40 Hz (TT). The standard errors of the averaged spectral densities are approximately 30%

of the maximum amplitude between 50 Hz and 90 Hz and increase to 38% above 80 Hz (MP); 30% of the maximum amplitude between 40 Hz and 55 Hz and increase to 58% above 50 Hz (LC); 30% of the maximum between 40 Hz and 55 Hz and increase to 88% above 45 Hz (MC); and 30% of the maximum between 25 Hz and 80 Hz and increase to 74% above 37 Hz (TT). In the auto-spectral density function at each of the four positions, the maximum standard error occurs at almost at the same frequency as the maximum amplitude of the auto-spectral density function. All auto-spectral density functions have peaks in a low-frequency range (between 30 Hz and 90 Hz). The shapes of these spectral density functions indicate the frequency components of the VAG signals at the four positions.

Fig. 5.3 shows the averaged cross-spectral density functions and standard error between the positions MP and the other three positions, namely LC, MC, and TT. As shown in Fig. 5.3(a), the cross-spectral density function of the VAG signals between the positions MP and LC has a peak at about 51 Hz and a bandwidth of approximately 23 Hz to 185 Hz; it decreases nonuniformly and reaches a value of about 90% of the maximum at around 51 Hz; the standard error is over 30% of the maximum amplitude between 40 Hz and 55 Hz and increases to 52% at 51 Hz. The cross-spectral density function of the VAG signals between MP and MC is given in Fig. 5.3(b), which has a peak at 44 Hz and a bandwidth of approximately 20 Hz to 140 Hz; it decreases nonuniformly and reaches a value of about 90% of the maximum at around 44 Hz; the standard error is over 30% of the maximum amplitude between 40 Hz and 85 Hz, and increases to 82% at 44 Hz. The cross-spectral density function between the positions MP and TT is shown in Fig. 5.3(c), which has a peak frequency of about 51 Hz and a bandwidth of approximately 20 Hz to 135 Hz; it decreases nonuniformly and reaches a value of about 90% of the maximum at around 51 Hz;

the standard error is over 30% of the maximum amplitude between 25 Hz and 70 Hz and increases to 49% at 30 Hz. The cross-spectral density functions have a peak in a lower frequency range (between 40 Hz and 55 Hz) than the auto-spectral density functions, and increase or decrease rapidly near the peak frequency. Another obvious characteristic of the cross-spectral functions is that the frequencies at which the maximum amplitude and the maximum standard error occur are not exactly equal. These could be due to the characteristics of transmission of VAG signals in the human knee joint, which could be described directly by the frequency response functions.

The amplitude of the frequency response function in response to stimulation at the position MP are given in Fig. 5.4. As can be seen in Fig. 5.4(a), the average amplitude of the frequency response function between positions MP and LC exhibits the expected feature of attenuation with positive slope below 51 Hz and negative slope over 51 Hz; the amplitude of the frequency response function increases or decreases rapidly below 100 Hz. Over 200 Hz, the attenuation is small and changes slower. The bandwidth is about 5 Hz to 160 Hz, and the amplitude is higher than 1 between 35 Hz and 55 Hz. The standard error has its maximum value at 51 Hz (about 37% of the maximum amplitude of the frequency response function) and decreases quickly below or over this frequency. The average amplitude of the frequency response function between the positions MP and MC is given in Fig. 5.4(b); it has positive slope below 51 Hz and negative slope over 51 Hz; the amplitude of the frequency response function increases or decreases rapidly below 180 Hz. Over 200 Hz, the attenuation is small and changes slower. The bandwidth is about 5 Hz to 185 Hz, and the amplitude is higher than 1 around 51 Hz. The standard error has its maximum value at 51 Hz (about 73% of the maximum amplitude of the frequency response function) and decreases quickly below or over this frequency. The amplitude frequency response function between the positions MP and TT is shown in Fig. 5.4(c); it has positive slope below 30 Hz and negative slope over 30 Hz; the amplitude of the frequency response function increases or decreases rapidly below 160 Hz. Over 200 Hz, the attenuation is small and changes slower. The bandwidth is about 5 Hz to 165 Hz, and the amplitude is higher than 1 from 20 Hz to 155 Hz. The attenuation changes rapidly near 30 Hz , and then slowly between 35 Hz and 155 Hz. The standard error has its maximum value at 30 Hz (about 68% of the maximum amplitude of the frequency response function) and decreases quickly below or over this frequency.

All frequency response functions are distributed nonuniformly. The average results obtained for all of the patients tested indicate that, during VAG signal production by mechanical stimulation, the knee joint system behaves as a bandpass filter having a peak in the low-frequency range (between 30 Hz and 60 Hz). The shape of the frequency response function is important in explaining the differences between the power spectra of various VAG signals.

VAG signals in response to stimulation were recorded from two normal subjects as well. The number of normal subjects is too small to study the results statistically; however, an example of magnitude of the frequency response function of one normal subject is shown in Fig. 5.5. These functions have a low-frequency peak (at 51 Hz), with the dominant range being between 50 Hz and 150 Hz.

5.4.2 Cadaver VAG Signals

VAG signals were obtained from two cadaver knees by stimulating near the MP position. Examples of the frequency response functions of a cadaver VAG signal are shown in Fig. 5.6. The shapes of these functions are obviously flat between 50 Hz and 250 Hz, and no obvious peak with value more than 1 exists. The upper frequency of the cadaver knee seems to be higher than that of the living knee, which may be caused by the loss of body solution in the cadaver knee. However, the result of the cadaver study supports the observation that VAG signals from noisy knee movement have bandpass vibrational characteristics. Experiments with more cadaver knees are required in order to establish a detailed model for the frequency response function.

5.5 Discussion

Results obtained for the subjects tested indicate that, during VAG signal production by mechanical stimulation, the knee joint system behaves as a bandpass filter having a peak in a low-frequency range. These results seem to explain the observation that VAG signals from noisy knee movement have low-frequency vibrational characteristics [24]. The bandpass transmission characteristics of the VAG signals through the knee joint system are similar for the different recording positions. However, the location of the peak in the frequency response function and the bandwidth of the filter were observed to change with the type of stimulation. The fact that the type of mechanical stimulation induces modifications to the transmission characteristics implies that the frequency response function could also be used as an indicator of various types of knee pathology and the state of the knee joint system.

The most important finding of the study is that the acoustic properties of the knee joint system under the condition of external mechanical stimulation are similar across different transmission paths under study, being comparable to a complex bandpass filter. However, a wide variation in the estimated frequency response function has been noted in the study. This large variation has been reflected by the large standard errors as shown in Fig. 5.4, and can be explained by the variations in fat thickness, bone excess, and the type of the pathology of the subjects.

Most of the transmission characteristics derived exhibit frequency ranges where the amplitude of the frequency response function is more than 1. For the paths between MP and LC, and between MP and MC, this range is narrow and lies around 51 Hz. For the path between MP and TT, the range is wider; however, the obvious peak lies at 30 Hz. The peaks could indicate resonance in the knee joint. The mechanical structure and in vivo tissue properties could result in the knee joint having different natural responance frequencies for different transmission paths. The joint structure is most sophisticated between MP and TT, where the transmission path includes liquid besides bone and soft tissues.

A limitation in this study, however, exists in the fact that the stimulus provided does not have a wide bandwidth. It should be pointed out that care should be exercised in applying the results directly to real VAG problems, since the paths of signal transmission for the stimulation experiment and knee movement would be different and the production of the VAG signal during knee movement is more complex than this simple model. However, considerable insight can be gained in dealing with the estimation of frequency response functions with the simplified decoupled modeling and stimulation procedures as presented. More sophisticated system modeling with impulse-type mechanical stimulation is necessary to confirm the results.

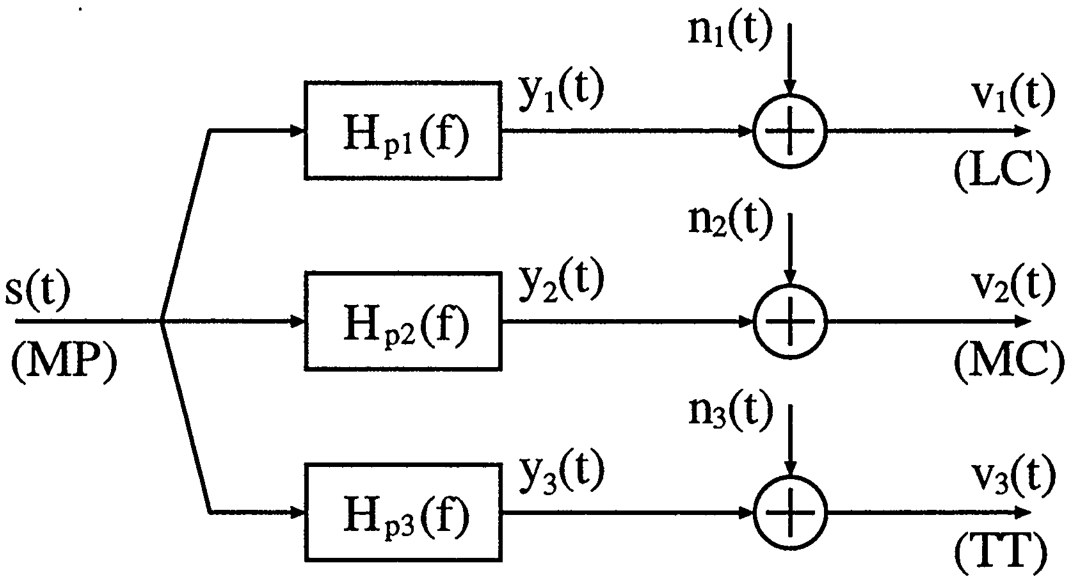

Figure 5.1 A basic model of the knee joint system with mechanical stimulation at mid-patella (MP).

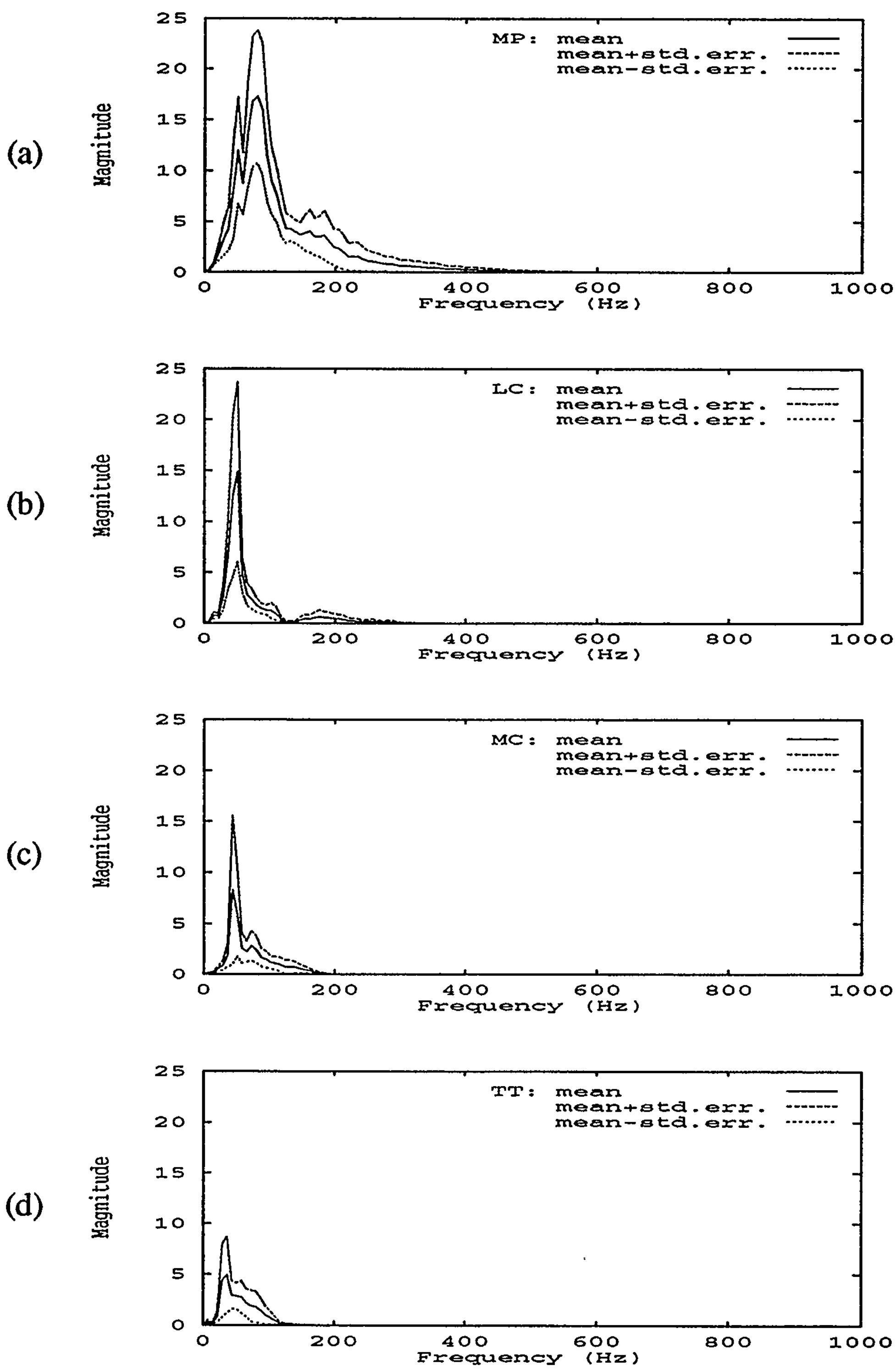

Figure 5.2 The average and standard error of input and output spectral density functions of VAG signals for 10 patients at various positions: (a) MP; (b) LC; (c) MC; and (d) TT.

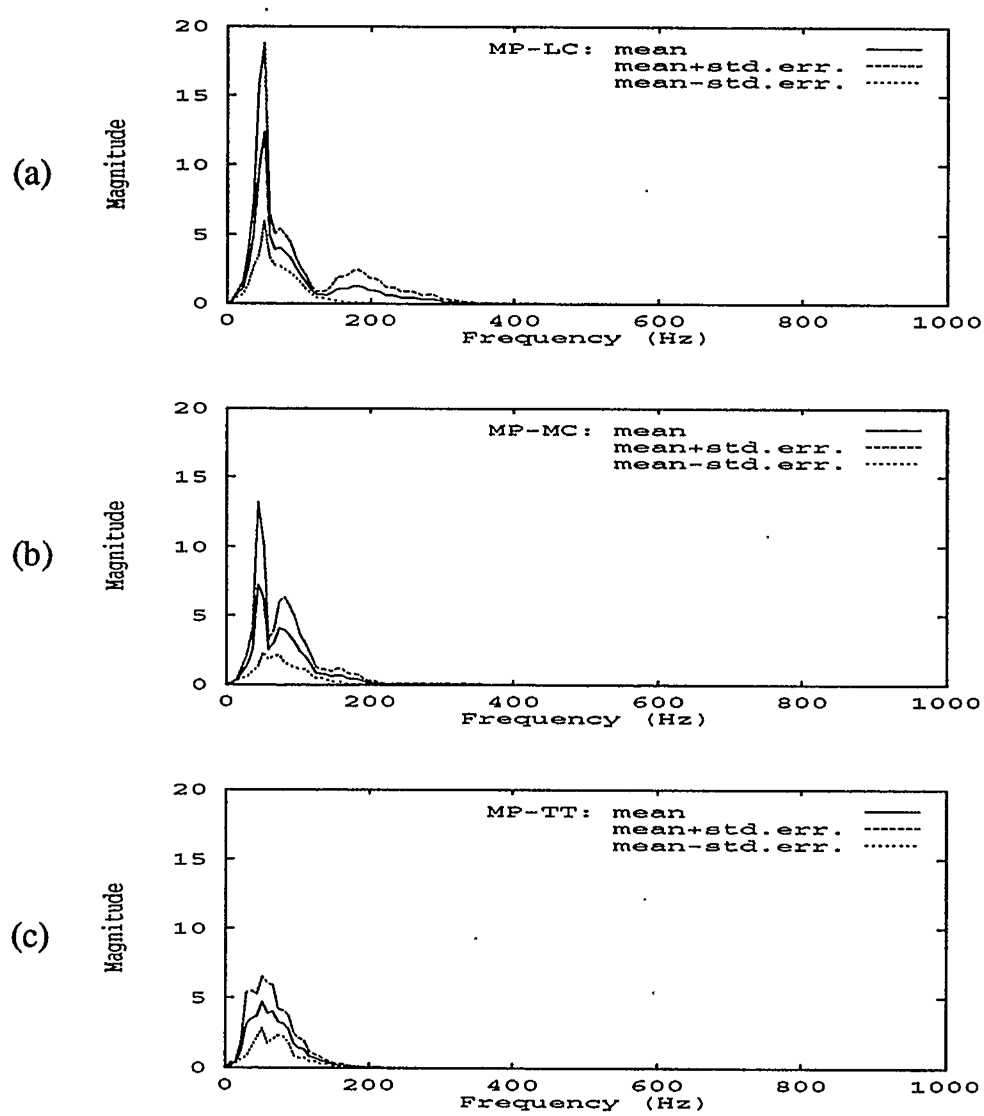

Figure 5.3 The average and standard error of cross-spectral density functions of VAG signals for 10 patients between (a) MP and LC; (b) MP and MC; (c) MP and TT.

(a)

(b)

(c)

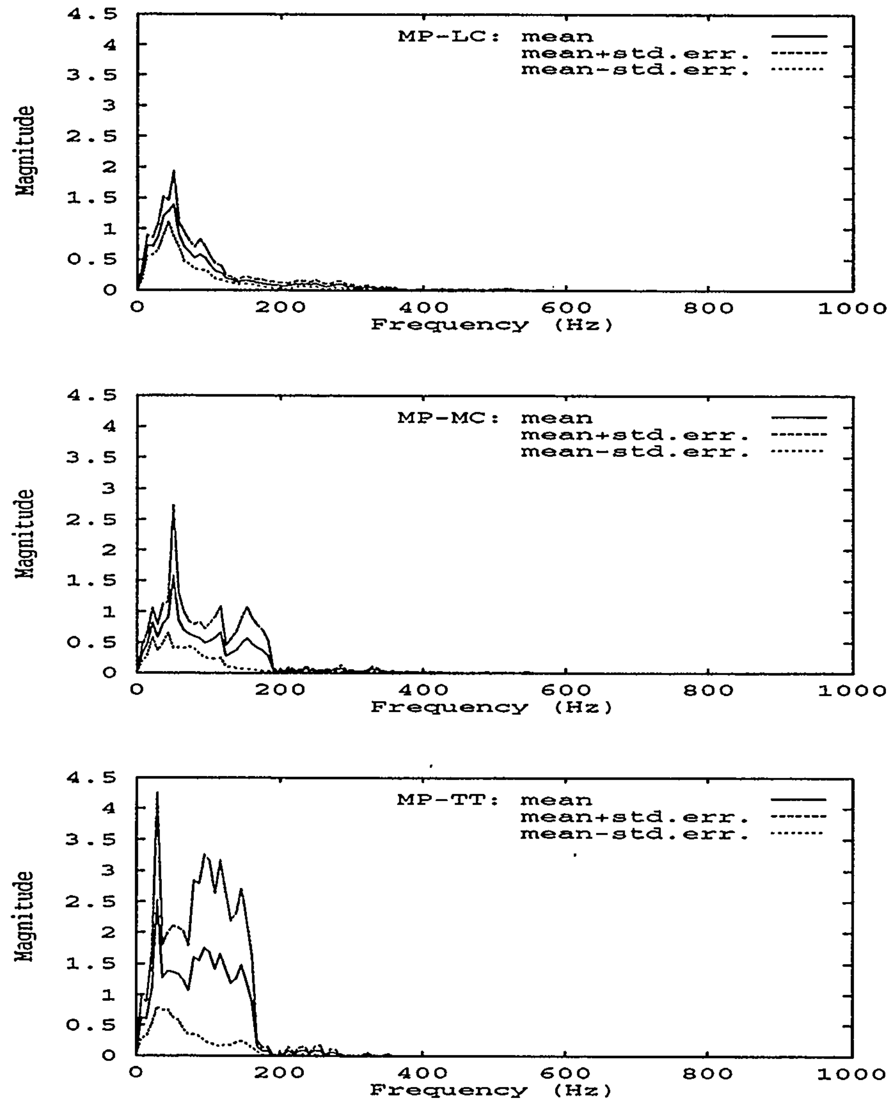

Figure 5.4 The average and standard error of the frequency response functions of VAG signals for 10 patients between: (a) MP and LC; (b) MP and MC; (c) MP and TT.

(a)

(b)

(c)

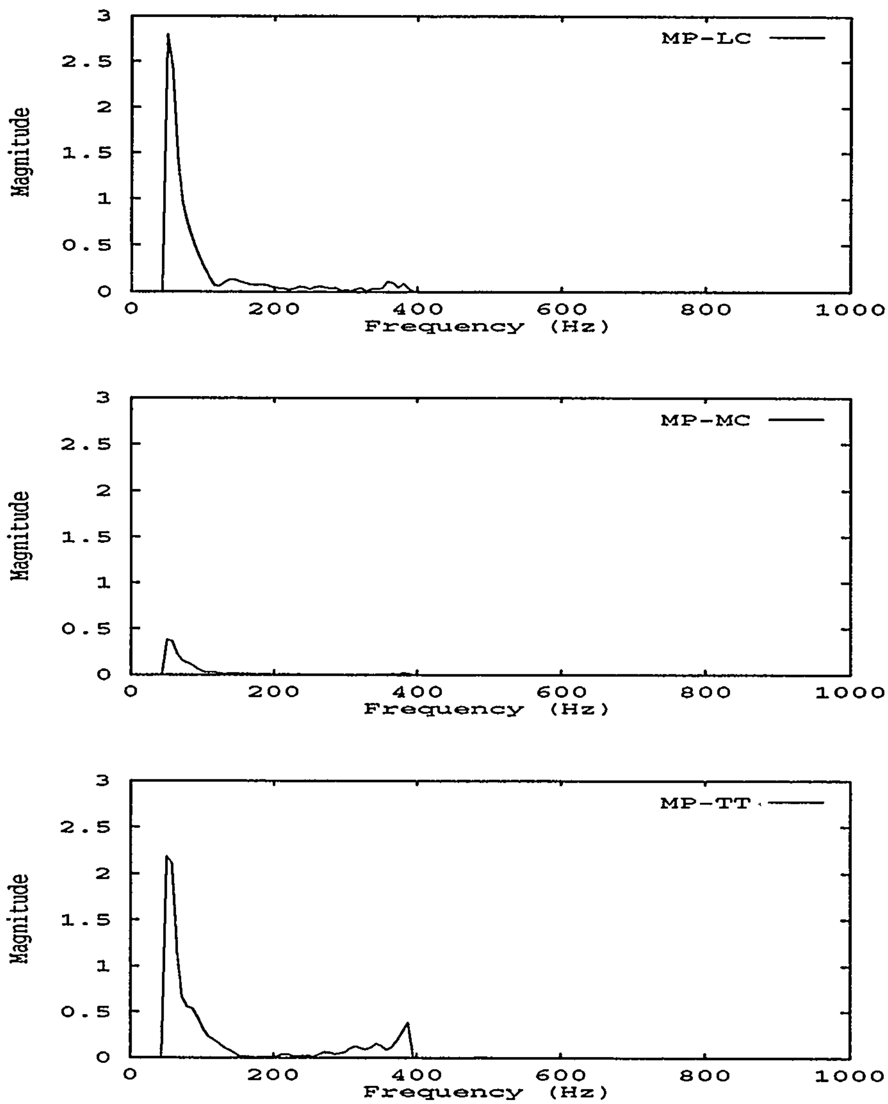

Figure 5.5 The frequency response functions of VAG signals for a normal subject between: (a) MP and LC; (b) MP and MC; (c) MP and TT. The corresponding VAG signals are illustrated in Fig. 2.2.

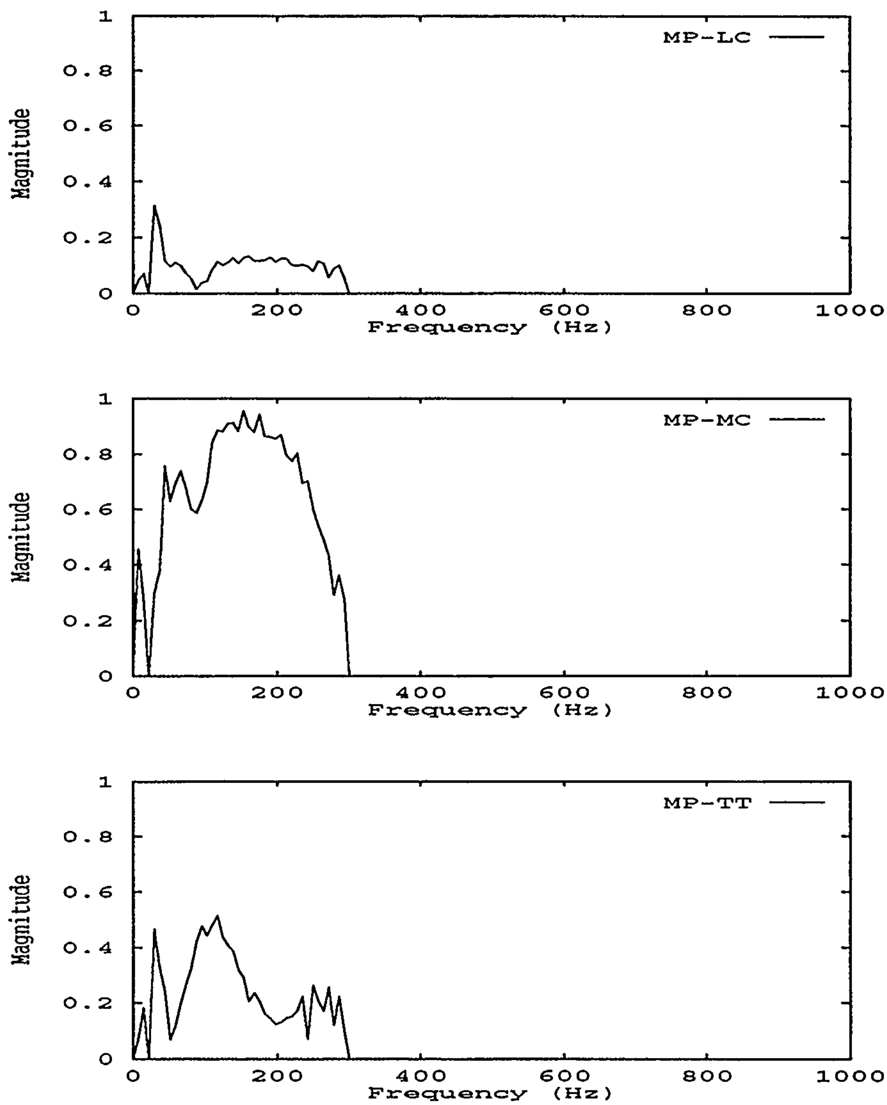

Figure 5.6 The frequency response functions of VAG signals of cadaver knee between: (a) MP and LC; (b) MP and MC; (c) MP and TT.

CHAPTER 6

TIME DELAY ANALYSIS FOR LOCALIZATION OF VAG SIGNALS

6.1 Introduction

VAG signals or joint sounds recorded over the surface of knee joints during flexion or extension may be associated with pathological conditions, such as meniscal tear and roughness caused by chondromalacia, in the knee joint [33, 19]. Correct and accurate source localization of such externally detected VAG signals may provide useful information concerning the part of the knee joint which is affected or injured. Information on the location of joint injury or disease is valuable in repair and surgery of knee joints and in monitoring of joint disease.

Many investigations have been carried out in the past few years on detection and analysis of knee vibrations or sounds, and the relation between VAG signals and knee pathology has been analyzed [33, 19]. However, most of these studies used single-channel signal analysis techniques, and consequently, could not indicate the location of the pathology.

With the availability of miniature accelerometers and multi-channel data acquisition systems, the potential exists for simultaneous multi-channel recording of knee joint VAG signals from a few locations over the joint. This chapter examines the possibility of localization of vibration sources within the natural or clinically relevant compartments of the knee joint using time delay analysis with multi-channel VAG data.

6.2 Methods

6.2.1 Subjects and Signal Recording

Fourteen subjects (2 normal subjects, 10 patients with knee pathology, and 2 cadavers) were investigated. The patients underwent arthroscopy after the VAG test.

VAG signals were recorded using a multi-channel vibration recording system with four miniature accelerometers (Dytran 3115a), which were placed over the skin surface at mid-patella (MP), lateral condyle (LC), medial condyle (MC), and tibial tuberosity (TT). Signals were conditioned with a bandpass filter of 10 Hz to 1 kHz and digitized at 15 kHz. Two kinds of VAG signals were tested: one generated by stimulating the joint with a single finger tap over the upperpole of the patella, and the other collected during knee movement at an angular velocity of approximately 4 seconds per swing.

In cadaver experiments, the knee was swung at the same velocity by a hydraulic actuator system, and signals were collected before and after lesions were created by a motorized arthroscopic shaver system.

6.2.2 Estimation of Source Location

Let $x_1(t)$ and $x_2(t)$ represent the VAG signals recorded at two different positions on the knee joint, and let us assume the underlying processes to be ergodic. A common method of estimating the time delay is by computing the cross-correlation function between the two signals $x_1(t)$ and $x_2(t)$ [71]:

$$\hat{R}_{x_1x_2}(\tau) = \frac{1}{T-\tau}\int_{\tau}^{T} x_1(t)x_2(t-\tau)dt, \tag{6.1}$$

where T denotes the observation interval and τ is the time shift between the signals. The cross-correlation function $\hat{R}_{x_1x_2}(\tau)$ of the nonperiodic VAG signals will have a peak in amplitude if a component of each VAG signal originates from a common source.

6.2.2.1 Model for Estimating the Source Location

A schematic representation of the model for source localization of VAG signals is shown in Fig. 6.1. $x_1(t)$, $x_2(t)$, $x_3(t)$, and $x_4(t)$ represent the signals after removal of the means from the raw VAG signals collected at the positions MP, LC, MC, and TT. There are six pairs of signals to be analyzed for time delay: MP and LC, MP and MC, MP and TT, LC and MC, LC and TT, and MC and TT. The cross-correlation of each pair of signals was calculated; the time delay between two locations corresponds to the peak in the corresponding cross-correlation function. The transducer position at which the VAG signal arrives the earliest is estimated to be the closest to the source location.

6.2.2.2 Signal Analysis

There are two basic approaches to the estimation of auto-correlation and cross-correlation functions. The first method is the standard approach of estimating the correlation function by direct computation of averaged products among the sample data values. The second method is the round-about approach of the first computing a power spectrum by direct Fourier transform procedures, and then computing the inverse Fourier transform of the power spectrum.

In this study, fast Fourier transform (FFT) computations were used to estimate the auto-correlation and cross-correlation functions. The double use of FFT procedures to compute both spectral density functions and the correlation functions can make this total operation more efficient than direct procedures. The following steps were used to compute the cross-correlation function via FFT procedures. The initial sample size for both $x_1(t)$ and $x_2(t)$ was set to be $N = 2^p$, where p is an integer. The cross-correlation function may be obtained from the cross-spectral density function and involves two separate FFTs, one for $x_1(t)$ and another for $x_2(t)$. These two FFTs may be computed simultaneously by using the method described below [71].

The signal data processing steps for removing non-zero mean value of raw VAG signal and computing the auto-spectral density function and cross-spectral density function are the same as the procedures described in section 5.3.2 (step $1-6$). After that, further computing steps are used as follows to obtain the auto-correlation function and cross-correlation function:

7. The auto-correlation is the real part of the inverse FFT of the magnitude of the auto-spectral density function; it is normalized by dividing by the value of the auto-correlation at $n = 0$.

8. The cross-correlation is the real part of the inverse FFT of the magnitude of the cross-spectral density function.

It was found necessary to apply a bandpass filter to each signal before the data processing procedures as above. The bandwidth of 300 Hz to 800 Hz filter was found to be suitable. Results of analysis with and without this filter will be compared in a later section.

The time delay between the two signals analyzed is the time shift corresponding to the maximum cross-correlation. After applying the above procedures to each of the six pairs of signals, the transducer position at which the VAG signal arrives the earliest is estimated to be the closest to the source location.

6.3 Results

6.3.1 Tap Signals

In earlier testing, an activator device was used to stimulate the knee joints of a few normal and abnormal subjects to elicit VAG signals. These signals could not be used as the activator device produced such strong signals that the recorded VAG signals were distorted.

VAG signals in response to a single finger tap at the patella were recorded from two normal subjects, ten patients, and two cadavers. The four-channel VAG data for subject B are shown in Fig. 2.2. The cross-correlations between the six pairs of signals for subject B are shown in Fig. 6.2. For this example, the time delays for the various pairs are: LC is delayed from MP (written as MP-LC) by 1.267 ms, MP-MC 43 ms, MP-TT 4.733 ms, LC-MC 12 ms, TT-LC 4.267 ms, and TT-MC 8.867 ms. Because LC, MC, and TT are all delayed with respect to MP, the source should be closest to the position of MP. This corresponds to the external stimulation position. Further, among LC, MC, and TT, the signal comes to TT earliest; between LC and MC, the signal arrival is earlier at LC.

For the 14 subjects studied, the results using cross-correlation were correct for 13 subjects. Similar results were obtained with or without use of the bandpass filter to pre-process the signals.

6.3.2 Swing Signals

The subjects mentioned above were asked to swing their legs at the angular speed of 4 seconds per swing. In the case of the cadavers, the leg was swung by an actuator device as described earlier. No VAG signals were observed for some subjects at some recording positions due to the transmission nature of the knee joints of the subjects. The VAG signals of only those subjects who had at least three channels of recordable signals are used in this study. Based on this requirement, the VAG signals of 9 patients, 2 normal subjects, and 1 cadaver knee were analyzed by the signal processing techniques. Table 6.1 presents the results of estimation of time delay for these cases by analyzing raw signals directly and after using a bandpass filter to pre-process the signals. The arthroscopy results for the patients and cadaver are shown in the table as well. The results for normal subjects are to be compared with the summary of auscultation findings listed in the table.

The first two cases (A and B) are normal subjects with normal noise and VAG signals occurring during swinging movement of the leg. The signals were estimated to be produced near the position of lateral condyle in case A and mid-patella in case B by auscultation. The results of time delay estimation agree with the auscultation reports.

Subjects C and D represent the two knees of the same cadaver tested using the multi-channel recording system. Before artificial lesions were made by arthroscopy, the right knee had mild degeneration of the tibial plateau and the lateral condyle, but these did not result in any VAG signals during swinging. In the left knee, there was mild chondromalacia of the patella, which also did not produce any signals; there was also degeneration of the tibial plateau that caused an obvious VAG signal at the tibial tuberosity.

No VAG signal was obtained from swing movement of the right knee after arthroscopy because the lesions made were too light to cause recordable VAG signals (case C). In the left knee, stronger lesions were cut on the surfaces of different parts in a step-by-step manner to get recordable VAG signals during swinging movement (case D).

The lesions on the patella were made in three steps: (1) medial patellar lesion; (2) lateral patellar lesion; and (3) central patellar lesion. The VAG signal source should be near the position of the transducer on the mid-patella for each of these lesions. The VAG signals recorded after cutting the first lesion were contaminated by noise with amplitude larger than those of the VAG signals. The VAG signals produced by the second and third lesions were used to analyze the source location. The cross-correlations of the signals for case D are shown in Fig. 6.3 (the raw VAG signals are shown in Fig. 2.4). The peak value of the cross-correlation function for each signal pair can be read from this figure. The precise data of the delays are: MP-LC 14.467 ms; MP-MC 3.6 ms; MP-TT 5.067 ms; MC-LC 39.133 ms; TT-LC 26.933 ms; and MC-TT 1.533 ms. The VAG signal arrives at the position of MP earliest, and thus the source should be closest to the mid-patella position.

Case E in table 6.1 is a patient who had medial meniscal tear and loose bodies between the patella and the tibia according to the arthroscopy report. These indicate the cause of sounds to be near the mid-patella and medial condyle, which are then transmitted to the other positions. The result based on cross-correlation and time delay estimation shows the source of the VAG signal to be on or closest to the mid-patellar area. The result was the same with or without the bandpass filter to pre-process the raw signals.

Case F had pathology of the anterior cruciate ligament, with the source of VAG signals estimated to be near the patella by arthroscopy. The result of analysis of the components of the VAG signal shows the source to be on or near the mid-patella. (The source was estimated in the wrong position, TT, without the bandpass filter.)

The subject G had medial meniscus tear, and the problem is on the medial condyle as reported by arthroscopy. The VAG signal source is on or closest to the medial condyle according to the estimation of delay time with or without using the bandpass filter to pre-process the VAG signals.

In case H, the patient had chondromalacia patella; the patella had severe damage and the lateral and medial condyles had light damage. The result based on time delay estimation is slightly different in that the source is estimated to be closest to the lateral condyle and second closest to the mid-patella; this could be due to the severest damage on the patella being near the lateral condyle.

The next four cases (I to L) also had correct results given by the signal processing techniques, as compared with the results of arthroscopy. Subject I had chondromalacia patella according to post-operative diagnosis, which showed light damage on the patella. This corresponds to the result of source localization by time delay estimation using the bandpass filter. (The source was wrongly estimated as TT without the filter.)

Case J had osteochondral fracture of the lateral condyle. Both the estimation of time delay and arthroscopy showed the VAG signal source to be on the lateral condyle.

The subject K had moderate damage on the tibial plateau and osteoarthritis on the lateral femoral condyle as diagnosed by arthroscopy; the result of signal analysis located the source as being around the tibial tuberosity.

Case L is a patient who had lateral chondromalacia and medial patella chondromalacia. The set of cross-correlation data for VAG signals during swinging for case L is shown in Fig. 6.4; the corresponding raw VAG signals are shown in Fig. 2.3. The delay time data are: LC-MP 2.667 ms; MP-MC 7.2 ms; MP-TT 7.6 ms; LC-MC 9.733 ms; LC-TT 9.933 ms; and MC-TT 1.133 ms. The VAG signal arrives at the transducer at the position of lateral condyle earliest based on these time delay data. This means that the VAG signal source should be closest to the position of lateral condyle. Indication of the source on the lateral condyle by analysis of the cross-correlation of the signals is a reasonable result.

The last patient, subject M, had a problem on the medial condyle as detected by time delay estimation with or without using the bandpass filter. This corresponds to the report of arthroscopy, which showed severe damage on the medial condyle.

6.4 Discussion

The cross-correlation functions of VAG signals were observed to have multiple peaks, which indicates that the VAG signals are not white noise signals and also that they cannot be represented by simple mathematical expressions. This could cause some difficulties in the analysis of the VAG signals.

The percentage of correct source localization for the VAG signals using mechanical stimulation is high (13/14, about 93%). The fact that the source is absolutely isolated and the transmission paths are simple makes the signals convenient to analyze.

The VAG signals recorded during swing movement are more sophisticated due to the complexity of the joint structure and the possibility of existence of multiple VAG components. Nine out of twelve (75%) of subjects had the correct location detected by the cross-correlation technique; the percentage of correct results increased to about 92% (11/12 cases) after using a bandpass filter to remove noise and interference which affect low-amplitude signals considerably. This promising result should be helpful in diagnosis and treatment of pathology of the knee joint.

A side-result of this study is that of estimating of the transmission velocity of VAG signals inside the knee joint or through the surface of the knee based on the time delay data. Suppose that the average distance between MP and LC is 6 cm; MP-MC 6 *cm*; and MP-TT 7.5 *cm*. The range of the propagation velocity of the VAG signal is then given to be from several m/s to several hundred m/s, which is between the propagation velocity of compression waves (*e.g.* at 10 Hz the velocity is about 1500 m/s) and the propagation velocity of shear waves (*e.g.* at 10 Hz the velocity is about 10 m/s) [72]. The range is wider than that reported for the transmission velocity of heart sounds (from several m/s to 100 m/s). This could be due to more bone being present in the knee joint than around the heart, and the fact that sound transmits faster in bone than in soft tissue. The result could also indicate that a source having an associated complicated movement could produce compression as well as shear waves. The three forms of transmission of vibratory energy might explain this result as well [38]: 1) as a compression wave traveling with the velocity of sound in tissue (about 1500 m/s); 2) as a transverse shear wave which travels much more slowly than sound; and 3) on the surface of the body as "surface waves" - a mixture of compression and shear waves - which travel at about the same speed as shear waves. Human soft tissue is nearly incompressible due to high water content. This leads to a much smaller propagation velocity for shear waves than for compression waves. Unlike the conditions encountered with geological vibrations, the distances between the sources and the measuring sites in the human knee are comparatively small, so that the two wave types cannot be separated and interact strongly. In view of this strong coupling, one can expect the propagation of vibrations to be much slower than in the case compression waves alone.

At high frequencies (higher than 500 Hz), the propagation velocities become so large that time delays due to transmission in the knee joint could be negligible and the damping quite large [72]. In view of this point and consideration of muscle contraction interference at low frequency and noise at high frequency, the bandpass filter range of 300 Hz to 800 Hz for pre-processing was chosen so as to analyze only selected components of the VAG signals. Such pre-filtering is a normal and necessary tool in signal processing, and is appropriate for VAG source localization based on the results that have been obtained.

A limitation exists in this study in the fact that the number of transducers used is not large enough to permit accurate detection of the position of the VAG sources. Further, only short segments of VAG signals corresponding to possibly isolated VAG components were processed. More sophisticated techniques have to be developed for processing multiple components within a VAG signal record and for localizing multiple sources at different positions inside knee joint.

Table 6.1 Summary of source localization experiments using the method of time delay estimation.

Subject	Knee	Source Location Estimated by Time Delay Analysis		Source Location Estimated by Arthroscopy (auscultation for normal subjects)
		Without Filter	With Filter	
A (Normal)	left	lateral condyle	lateral condyle	lateral condyle, patella (auscultation)
B (Normal)	right	patella	patella	patella (auscultation)
C (cadaver)	right	no signal	no signal	patella
D (cadaver)	left	patella	patella	patella
E (patient)	right	patella	patella	patella, medial condyle
F (patient)	right	tibial tuberosity	patella	patella
G (patient)	left	medial condyle	medial condyle	medial condyle
H (patient)	right	medial condyle	lateral condyle	patella
I (patient)	right	tibial tuberosity	patella	chondromalacia patella
J (patient)	left	lateral condyle	lateral condyle	lateral femoral condyle
K (patient)	left	tibial tuberosity	tibial tuberosity	tibial plateau, lateral femoral condyle
L (patient)	right	lateral condyle	lateral condyle	lateral chondromalacia, medial patella chondromalacia
M (patient)	right	medial condyle	medial condyle	medial condyle

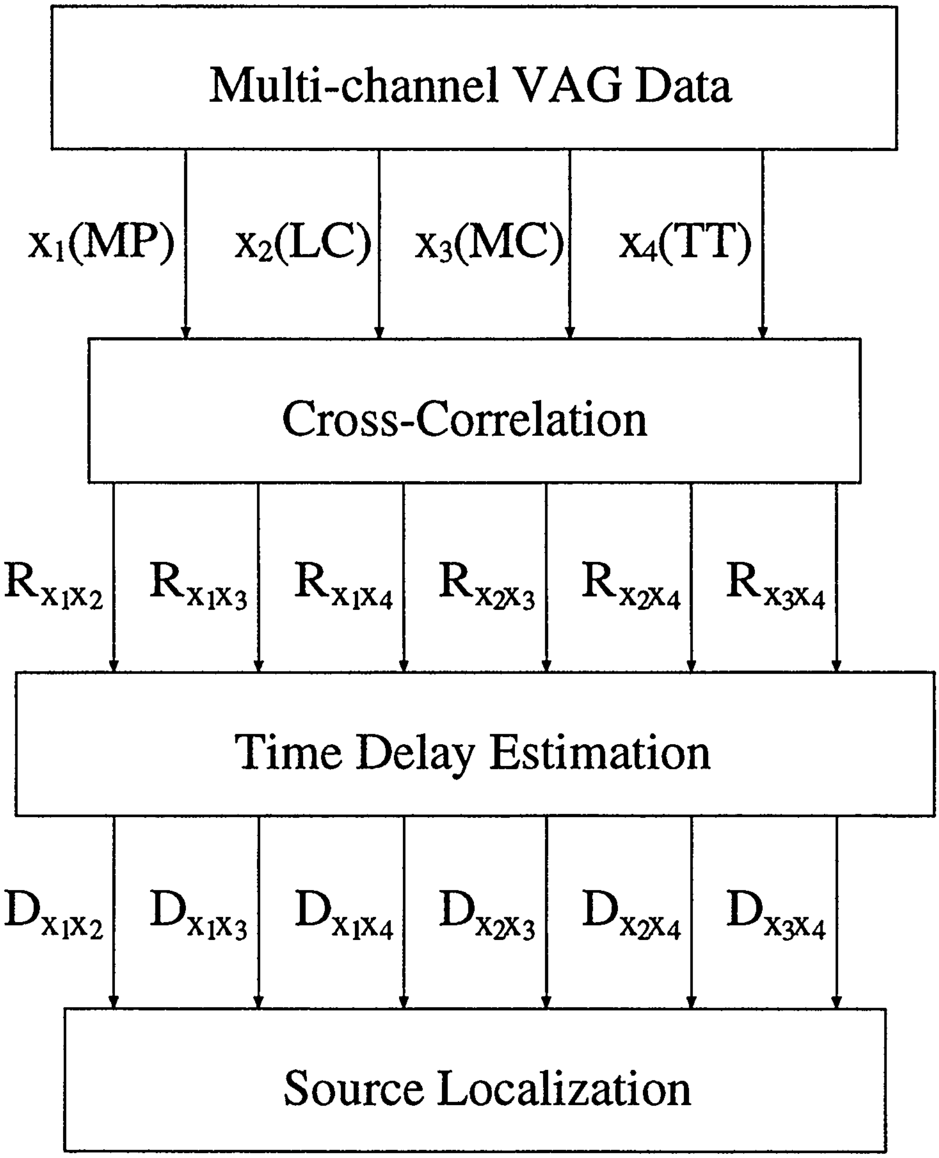

Figure 6.1 Model for source localization of VAG signals.

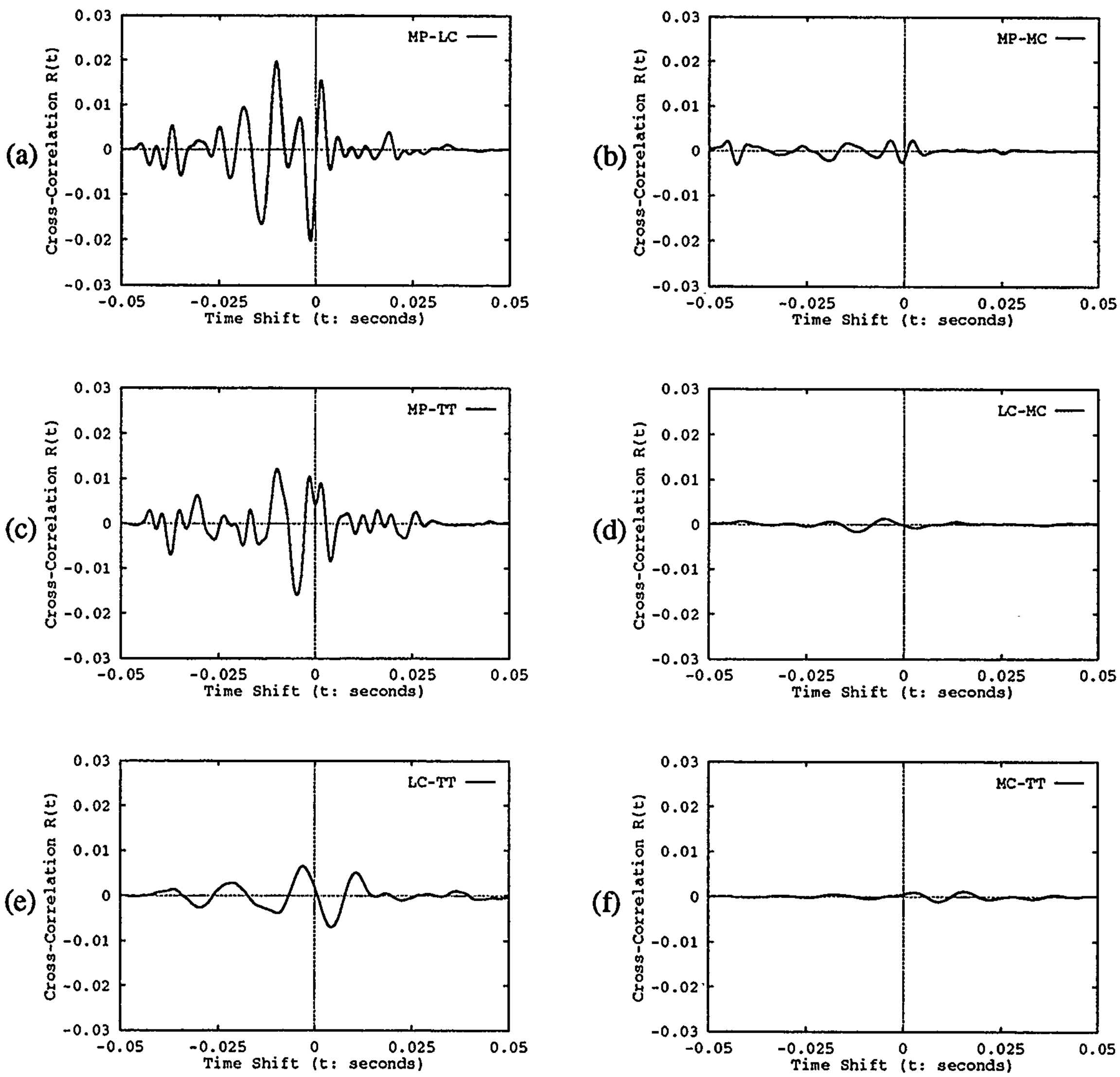

Figure 6.2 Cross-correlation functions of VAG signals obtained by finger tap from normal subject B. The corresponding VAG signals are illustrated in Fig. 2.2. (Note: t represents the time shift τ in the text.)

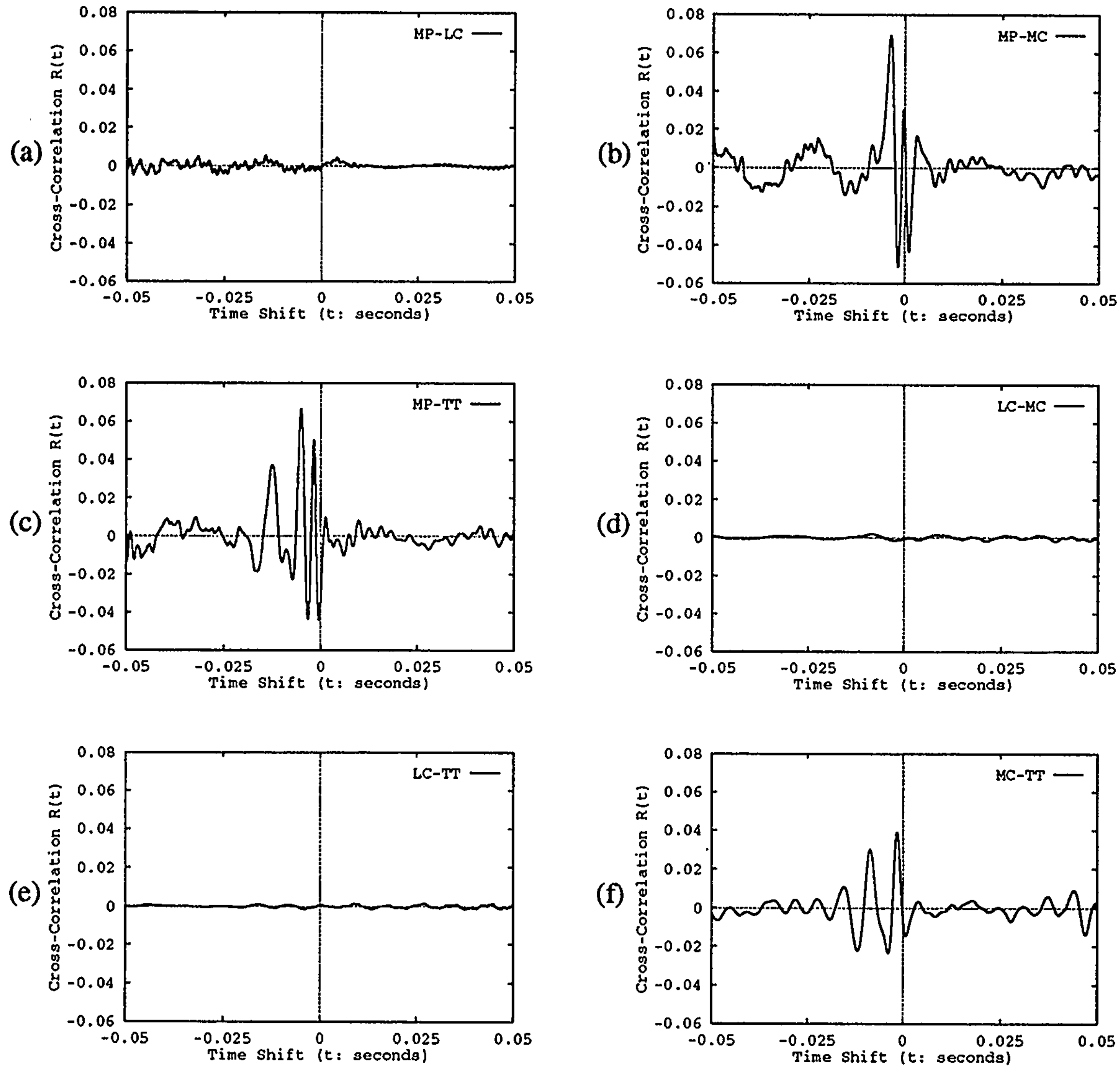

Figure 6.3 Cross-correlation functions of VAG signals during swinging movement from the left knee of a cadaver with lesions near the mid-patella (case D). The corresponding VAG signals are illustrated in Fig. 2.4. (Note: t represents the time shift τ in the text.)

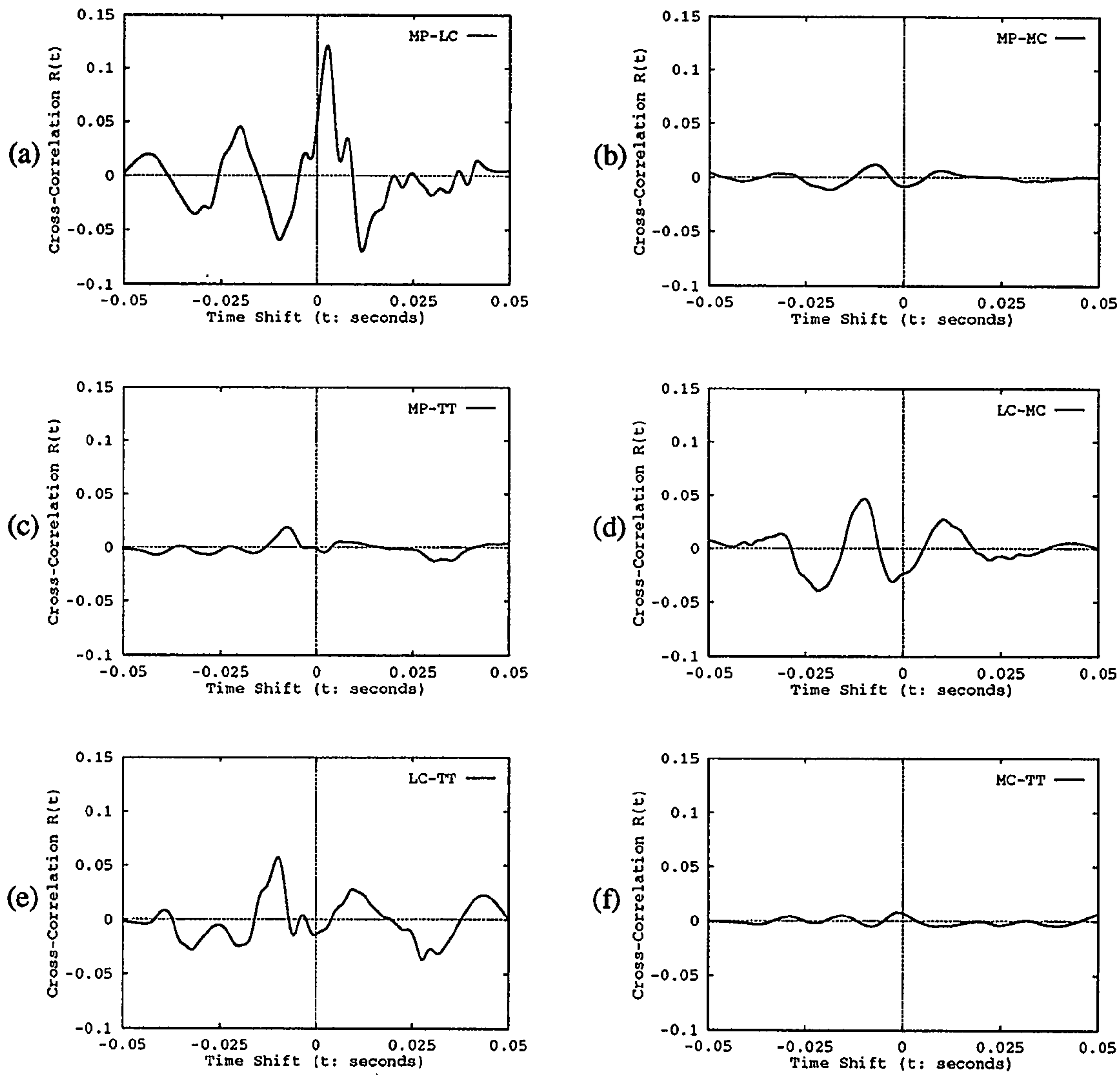

Figure 6.4 Cross-correlation functions of VAG signals during swinging movement from a patient with lateral chondromalacia and medial patella chondromalacia (case L). The corresponding VAG signals are illustrated in Fig. 2.3. (Note: t represents the time shift τ in the text.)

CHAPTER 7

CONCLUSIONS AND FUTURE WORK

The potential use of time delay estimation in source localization of knee vibration (VAG) signals was studied in this thesis. The method of cross-correlation was used successfully to estimate the time delay between pairs of VAG signals. A bandpass filter was found to be useful in pre-processing signals to extract VAG signal components suitable for time delay analysis. Cross-correlation functions were analyzed and their peaks were detected to determine time delays. Time delays between six pairs of signals (from four VAG signals recorded simultaneously) were used to estimate the source locations of VAG signals. Arthroscopy (auscultation in the cases of normal volunteers) was used to verify the results of source localization. Results obtained from the analysis of signals of 2 normals, 9 patients, and 2 cadavers (2 for tap signals and 1 for swing signal) suggest that the method has good potential in localizing the sources of knee VAG signals at different positions within the knee.

The transmission of VAG signals was studied in this thesis as well by using basic models of frequency response functions. Frequency spectra were used to determine the frequency response functions of VAG signal transmission paths. The average results obtained for the all of the patients studied indicate that the knee joint system behaves as a bandpass filter having a peak in the low-frequency range of 30 Hz to 60 Hz. Frequency response functions for normal subjects and different degenerated knees should be investigated further as they may provide useful information to distinguish abnormal knees from normal knees.

Estimation of the velocity of VAG signal transmission in the human knee was a side-product of this work. The estimated velocities were in the range of several to several hundred m/s, suggesting the existence of a mixture of shear and compression waves. Further study of transmission speeds of different frequency components could be useful in describing the transmission characteristics of VAG signals and in source localization.

The number of normal and cadaver subjects available was limited (2 each), although a better number of patients with cartilage pathology (9) was included in the study. Confirmation of the results obtained will require analysis of signals from more subjects.

More sophisticated system modeling with impulse-type mechanical stimulation is recommended for further studies on the transmission of VAG signals in the human knee.

This thesis has established the viability of multi-channel VAG signal analysis for source localization and characterization of the transmission of VAG signals. It is hoped that this work will lead to a non-invasive diagnostic and treatment procedure for human knee joint pathology.

REFERENCES

[1] R.W. Jackson and I. Abe. The role of arthroscopy in the management of disorders of the knee: An analysis of 200 consecutive examinations. *J. Bone Joint Surgery. (Brit.)*, 54-B:310–322, 1972.

[2] V.H. Frankel and M. Nordin, editors. *Basic Biomechanics of the Skeletal System.* Lea & Febiger, Philadelphia, 1980.

[3] After arthroscopy: Regaining your full knee potiential. Booklet, Krames Communications, 1990.

[4] D.N. Kulund, editor. *The Injured Athlete.* J.B.Lippincott Company, Philadelphia, 2nd edition, 1988.

[5] S.G. Edward, J.S. Wilfredo, R.N. Frank, and L.B. David. Biomechanics of the knee-extension exercise. *Bone and Joint Surgery*, pages 725–733, 1984.

[6] D.S. Hungerford and M. Barry. Biomechanics of the patellofemoral joint. *Clinical Orthopaedics*, 144:9–15, 1979.

[7] W.G. Kernohan and R.A.B. Mollan. Processing of sound signals in orthopaedic surgery. In *Proc. 2nd European Signal Processing Conf. (EUSIPCO-83)*, page 581, Amsterdam, 1983.

[8] W.E. Blodgett. Auscultation of the knee joint. *Boston Medical and Surgical Journal*, 146(3):63–66, 1902.

[9] E. Bircher. Zur diagnose der meniscusluxation und des meniscusabrisses. *Zentralbl.Chir*, 40:1852–1857, 1913.

[10] C.F. Walters. The value of joint auscultation. *Lancet*, 1:920–921, 1929.

[11] K.H. Erb. Uber die moeglichkeit der registrierung von gelenkgeraeuschen. *Deutsche Z. Chir*, 241:237–245, 1933.

[12] A. Steindler. Auscultation of the joints. *J. Bone and Joint Surgery*, 19:121–124, 1937.

[13] A. Peylan. Direct auscultation of the joints (preliminary clinical observations). *Rheumatism*, 9:77–81, 1953.

[14] H. Fischer and E.W. Johnson. Analysis of sounds from normal and pathologic knee joints. In *3rd Int. Congr. Phys. Med*, pages 50–57, 1960.

[15] E. Szabo, L. Danis, and Z. Torok. Examination of the acoustic phenomena observed in the knee. *Traumatologia*, 15(2):118–127, 1972.

[16] M.L. Chu, I.A. Gradisar, M.R. Railey, and G.F. Bowling. Detection of knee joint diseases using acoustical pattern recognition technique. *J. Biomechanics*, 9:111–114, 1976.

[17] M.L. Chu, I.A. Gradisar, L.D. Zavodney, and G.F. Bowling. Computer-aided acoustical correlation of pathological cartilage-generated noise. In *30th Annual Conference on Engineering in Medicine and Biology*, page 175, Nov 1977.

[18] M.L. Chu, I.A. Gradisar, M.R. Railey, and G.F. Bowling. An electro-acoustical technique for the detection of knee joint noise. *Medical Research Engineering*, 12(1):1820, 1976.

[19] M.L. Chu, I.A. Gradisar, and R. Mostardi. A noninvasive electroacoustical evalution technique of cartilage damage in pathological knee joints. *Medical & Biological Engineering & Computing*, 16:437–442, 1978.

[20] R.A.B. Mollan, G.C. McCullagh, and R.I. Wilson. A critical appraisal of auscultation of human joints. *Clinical Orthopaedics and Related Research*, 170:231–237, 1982.

[21] G.W. Kernohan, D.E. Beverland, G.F. McCoy, S.N. Shaw, R.G.H. Wallace, G.C. McCullagh, and R.A.B. Mollan. The diagnostic potential of vibration arthrography. *Clinical Orthopaedics and Related Research*, pages 106–112, 1986.

[22] W.G. Kernohan and R.A.B. Mollan. Microcomputer analysis of joint vibration. *J. Microcomputer Applications*, 5:287–296, 1982.

[23] D.E. Beverland, G.F. McCoy, W.G. Kernohan, and R.A.B. Mollan. What is patellofemoral crepitus? *J. Bone and Joint Surgery*, 68-B:496, 1986.

[24] G.F. McCoy, J.D. McCrea, D.E. Beverland, W.G. Kernohan, and R.A.B. Mollan. Vibration arthrography as a diagnostic aid in disease of the knee. *J. Bone and Joint Surgery*, 69-B(2):288–293, 1987.

[25] G.F. McCoy, D.E. Beverland, W.G. Kernohan, A. Agahi, and R.A. Mollan. Vibration arthrography in knee joint diseases. In *Eighth Combined meeting of the Orthopaedic Associations of the English-speaking World*, page Paper No. 8, The American Orthopaedic Association, Washington, D.C., May 1987.

[26] W. Mang, M. Birk, and G. Blumel. Practical application of phonoarthrography in the diagnosis of knee joint disease. *Z. Orthop.*, 118(1):85–90, 1980.

[27] J. Inoue, Y. Nagata, and K. Suzuki. Measurement of knee joint sounds by microphone. *Sangyo Ika Daigaku Zasshi*, 8(3):307–316, 1986.

[28] Y. Nagata, K. Suzuki, Y. Kobayashi, M. Sasaki, J. Inoue, and H. Takyu. Joint-sounds clinical experience of the knee joint. *Sangyo Ika Daigaku Zasshi*, 8:425–428, 1986.

[29] R.M. Rangayyan, C.B. Frank, G.D. Bell, and R. Smith. Analysis of knee joint sound signals. In *Proc. IEEE Engineering in Medicine and Biology Society 10th Annual International Conf.*, pages 712–713, 1988.

[30] Y.T. Zhang, K.O. Ladly, R.M. Rangayyan, C.B. Frank, and G.D. Bell. Muscle contraction interference in acceleration vibroarthrography. In *Proc. IEEE Engineering in Medicine and Biology Society 12th Annual International Conf.*, pages 2150–2151, Philadelphia, 1990.

[31] Y.T. Zhang, K.O. Ladly, Z.Q. Liu, S. Tavathia, R.M. Rangayyan, C.B. Frank, and G.D. Bell. Interference in displacement vibroarthrography and its adaptive cancellation. In *Proc. Canadian Medical and Biological Engineering Society Conf.*, pages 107–108, Winnipeg, June 1990.

[32] K.O. Ladly. Analysis of patellofemoral joint vibration signals. Master's thesis, The University of Calgary, AB, Canada, 1992.

[33] S. Tavathia, R.M. Rangayyan, C.B. Frank, G.D. Bell, K.O. Ladly, and Y.T. Zhang. Analysis of knee vibration signals using linear prediction. *IEEE Trans. on BME*, 39(9):959–970, 1992.

[34] Z.K. Moussavi, R.M. Rangayyan, C.B. Frank, G.D. Bell, K.O. Ladly, and Y.T. Zhang. Statistical analysis of vibroarthrographic signals using the adaptive least squares method. In *Proc. of the Canadian Medical & Biological Engineering Society Conf.*, pages 96–97, Ottawa, Ontario, May 1993.

[35] L.E. Kinsler, A.R. Frey, A.B. Coppens, and J.V. Sanders, editors. *Fundamentals of Acoustics.* John Wiley & Sons, New York, 3nd edition, 1982.

[36] H.E. von Gierke. Transmission of vibratory energy through human tissue. In O. Glasser, editor, *Medical Physics*, volume 3, page 661. Year Book Medical, Chicago, 1960.

[37] D.E. Goldman and T.F. Hueter. Tabular data of the velocity and absorption of high-frequency sound in mammalian tissue. *J. Acoustic. Soc. Am.*, 28:35–37, 1956.

[38] J.J. Faber and A.C. Burton. Spread of heart sounds over the chest wall. *Circ Res*, 11:96–107, 1962.

[39] J.J. Faber. Origin and conduction of the mitral sound of the heart. *Circ Res*, 14:426–435, 1964.

[40] P. Heintzen and K.W. Vietor. The diacardiac phonocardiogram. *Am Heart J*, 65:59–67, 1963.

[41] R. Zalter, H.C. Hardy, and A.A. Luisada. Acoustic transmission characteristics of the thorax. *J Appl Physiol*, 18:428–436, 1963.

[42] G.A. Feruglio. An intracardiac sound generator for the study of the transmission of heart murmurs in man. *Am Heart J*, 63:232–238, 1962.

[43] D. Smith, T. Ishimitsu, and E. Craige. Mechanical vibration transmission characteristics of the left ventricle: implications with regard to auscultation and phonocardiography. *JACC*, 4(3):517–521, 1984.

[44] V.K. Iyer, P.A. Ramamoorthy, Y. Ploysongsang, and H. Fan. Reduction of heart sounds from lung sounds by adaptive filtering. *IEEE Trans. on BME*, BME-33:1141–1148, 1986.

[45] V.K. Iyer, P.A. Ramamoorthy, and Y. Ploysongsang. Autoregressive modeling of lung sounds: Characterization of source and transmission. *IEEE Trans. on BME*, 36(11):1133–1137, 1989.

[46] B.C. Kuo, editor. *Automatic Control Systems.* Prentice-Hall, Inc., Englewood Cliffs, New Jersey, fifth edition, 1987.

[47] L.G. Durand, J. Genest, and R. Guardo. Modeling of the transfer function of the heart-thorax acoustic system in dogs. *IEEE Trans. on BME*, BME-32(8):592–601, August 1985.

[48] C.H. Knapp and G.C. Carter. The generalized correlation method for estimation of time delay. *IEEE Trans. Acoust., Speech, Signal Processing*, 24(4):320–327, 1976.

[49] H.Q. Azizul. An overview on the time delay estimation in active and passive systems for target localization. *IEEE Trans. Acoust., Speech, Signal Procassing*, 29(3):527–533, 1981.

[50] F.A. Reed, P.L. Feintuch, and N.J. Bershad. Time-delay estimation using the LMS adaptive filter-static behavior. *IEEE Trans. Acoust., Speech, Signal Processing*, ASSP-29:561–568, 1981.

[51] D.H. Youn, N. Ahmed, and G.C. Carter. On using the LMS algorithm for delay estimation. *IEEE Trans. Acoust., Speech, Signal Processing*, ASSP-30:798–801, 1982.

[52] D. Boudreau and P. Kabal. Joint time-delay estimation and adaptive recursive least squares filtering. *IEEE Trans. on Signal Processing*, 41(2):592–601, 1993.

[53] D.M. Etter and S.D. Stearns. Adaptive estimation of time delay in sampled data systems. *IEEE Trans. Acoust., Speech, Signal Processing*, 29(3):582–587, 1981.

[54] P.R. Roth. How to use the spectrum and coherence function. *Sound and Vibration*, 5(1):10–14, 1971.

[55] A.C. Eberhardt and W.F. Reiter. Application of the coherence function in truck noise analysis. In *Proc. of Symposium on University Research in Transportation Noise*, pages 520–532, 1974.

[56] Y. Ishii and M. Ishida. Application of cross-spectral analysis to the measurement of contribution of noise sources. Report 493, Institute of Space and Aeronautical Science, University of Tokyo, 1973.

[57] L.D. Enochson. Frequency response function and coherence function for multiple input linear systems. Report CR-32, NASA, 1964.

[58] L.L. Koss and R.J. Alfredso. Identification of transient sound sources on a punch press. *J. Sound Vib.*, 34(1):11–38, 1974.

[59] K.W. Goff. The application of correlation techniques to some acoustic measurements. *J. Acoust. Soc. of Am.*, 27(2):236–246, 1954.

[60] T.E. Siddon. Noise generating mechanisms for passenger car tires. In *Proc. of Meeting of Acoustical Society*, pages 62–73, Miami, FL, USA, 1971.

[61] C.B. Pease. Experience with simple uses of correlation technique in acoustics. Report, National Gas Turbine Establishment, Pyestock, England, 1971.

[62] W.R. Hahn. Optimum signal processing for passive sonar range and bearing estimation. *J. Acoust. Soc. Am.*, 58(1):201–205, 1975.

[63] G.C. Carter. Time delay estimation for passive sonar signal processing. *IEEE Trans. on Acoustics, Speech, and Signal Processing*, ASSP-29(3):463–470, 1981.

[64] C.H. Joseph. Passive bearing estimation of a broad-band source. *IEEE Trans. on Acoustics, Speech, and Signal Processing*, ASSP-32(2):426–431, 1984.

[65] W.A. Gardner and C. Chen. Signal-selective time-difference-of-arrival estimation for passive location of man-made signal sources in highly corruptive environments. *IEEE Trans. on Signal Processing*, 40(5):1168–1197, 1992.

[66] W.A. Hahn and S.A. Tretter. Optimum processing for delay-vector estimation in passive signal arrays. *IEEE Trans., Information Theory*, 19:608–613, 1973.

[67] Y.P. Shen, R.M. Rangayyan, C.B. Frank, G.D. Bell, and Y.T. Zhang. Time delay estimation for source localization of vibroarthrographic signals from human knee joints. In *Proc. of the 15th Annual International Conf. of the IEEE Engineering in Medicine and Biology Society*, pages 381–382, San Diego, California, USA, October 1993.

[68] C.B. Frank, R.M. Rangayyan, and G.D. Bell. Analysis of knee joint sound signals for noninvasive diagnosis of cartilage pathology. *IEEE Engineering in Medicine and Biology Magazine*, pages 65–68, 1990.

[69] W.G. Kernohan, D.E. Beverland, G.F. McCoy, A. Hamilton, P. Watson, and R.A.B. Mollan. Vibration arthrometry. *Acta Orthop Scand*, 61(1):70–79, 1990.

[70] Y.T. Zhang, C.B. Frank, G.D. Bell, Y.P. Shen, and R.M. Rangayyan. Vibroarthrographic transfer function of the knee joint system during mechanical stimulation. In *Canadian Medical & Biological Engineering Society*, pages 364–365, Ottawa, Ontario, Canada, May 1993.

[71] J.S. Bendat and A.G. Piersol, editors. *Random Data: Analysis and Measurement Procedures*. John Wiley & Sons, New York, 2nd edition, 1986.

[72] L.H. van der Tweel and J. Verburg. Physical concepts. In R.S. Reneman and J. Strackee, editors, *Data in Medicine: Collection, Processing and Presentation*, pages 11 – 51. Martinus Nijhoff Publishers, The Hague, 4th edition, 1979.